1

Rotor Aerodynamic Theory

1.1 Introduction

Theoretical background in energy extraction generalities and, more specifically, rotor aerodynamics of horizontal axis wind turbines (HAWTs) is developed in this chapter. Some prior knowledge of fluid dynamics in general and as applied to the analysis of wind turbine systems is assumed, in particular basic expressions for energy in a fluid flow, Bernoulli's equation, definitions of lift and drag, some appreciation of stall as an aerodynamic phenomenon and blade element momentum (BEM) theory in its conventional form as applied to HAWTs. Nevertheless, some of this basic knowledge is also reviewed, more or less from first principles. The aim is to express particular insights that will assist the further discussion of issues in optimisation of rotor design and also aid evaluation of various types of innovative systems, for example, those that exploit flow concentration.

Why focus much at all on theory in a book about innovative technology? Theory is often buried in more or less opaque computer code, which may generate loads of information that engineers can use in design. However, as is amplified in the following chapters, theory is in itself:

- Food for innovation and suggestive of methods of performance enhancement or alternative concepts;
- A basis for understanding what is possible and providing an overview appraisal of innovative concepts;
- A source of analytic relationships that can guide early design at a stage where many key parameters remain to be determined and there are too many options to subject each to detailed evaluation.

Prior to discussions of actuator disc theory and the BEM theory that has underpinned most practical engineering calculations for rotor aerodynamic design and determination of wind turbine loads, some discussion of aerodynamic lift is presented. This is intended particularly to highlight a few specific insights which can guide design and evaluation of wind energy systems. In general, a much more detailed understanding of basic aerodynamics is required in wind turbine design. This must cover a wide range of topics, 2D and 3D flow effects in relation to aerofoil performance, stall behaviour, aeroelastic behaviour, unsteady effects including stall hysteresis and induction lag, determination of suitable aerofoil data for wide ranges in angle of attack, and so on. References [1–10] are a sample from extensive published work covering some of these issues.

Innovation in Wind Turbine Design, Second Edition. Peter Jamieson.

1.2 Aerodynamic Lift

The earliest wind turbines tended to use the more obvious drag forces [11] experienced by anyone exposed to wind on a windy day, and use of the potentially more powerful lift forces was almost accidental. Exploitation of the aerodynamic lift force is at the heart of efficient modern wind turbines, but surprisingly the explanation of lift has been quite contentious. Before entering that territory, consider first Bernoulli's equation which is derived in many standard sources on fluid mechanics. Ignoring gravitational, thermal and other energy sources and considering only pressure and kinetic energy, this equation becomes: $p + 1/2\rho U^2 = p_0$, where p is static pressure in a fluid element moving with a velocity of magnitude U, ρ is fluid density and p_0 is the total pressure which, in the absence of energy extraction, is constant along any streamline in the flow field.

Bernoulli's equation is essentially an energy equation expressed dimensionally in units of pressure and can be viewed as conservation of energy per unit volume of the fluid. In that connection, pressure can be regarded as the source potential energy (per unit volume) that drives fluid flow. This interpretation is discussed subsequently and is seen to be crucial to a clear understanding of how a wind turbine rotor works.

Returning to the issue of aerodynamic lift, one view of the explanation of the lift force has been that the fluid, should it have a longer path to traverse on one side of an aerofoil, will travel faster in order to meet the fluid flowing past the other side at the trailing edge of the aerofoil. With increase in velocity, the associated static pressure in that region will reduce in consequence of Bernoulli's equation. The pressure deficit on the side of the plate with the longer flow path is then considered the source of the lift force.

There are various problems with this as an explanation of the lift force. Firstly, a thin plate set at an angle in a uniform flow field will generate significant lift when, considering its shape, there is negligible difference between the upper surface and lower surface paths. Secondly, if an aerofoil with a shape with a noticeably longer flow path on one side is considered and the assumption that the flow on each side will traverse the length of the aerofoil in equal times (something that in itself can be challenged) is made, the difference in static pressure calculated on the basis of the implied velocities on each side of the aerofoil will be found quite insufficient to account for the observed lift force.

An apparently authenticated story relates to the efforts of the famous physicist Albert Einstein in aerofoil development. Einstein's effort, inspired by the path-length-related concept, was a miserable failure[1] and he later commented '*That is what can happen to a man who thinks a lot but reads little.*'

---

1 According to Carl Seelig (*Albert Einstein: A Documentary Biography* by Carl Seelig, 1960, pp. 251–252; Translated by Mervyn Savill, London: Staples Press, Bib ID 2263034), an accredited biographer of Einstein: 'It is not well known that … Einstein … undertook a new aerofoil design intended for serial production. Eberhard, the chief test pilot, treated the fruit of the famous theoretician's efforts with suspicion.' 'Ehrhardt's letter continues (EA 59–556, as quoted in Folly 1955): A few weeks later, the "cat's back aerofoil" had been fitted to the normal fuselage of a LVG biplane, and I was confronted with the task of testing it in flight. … I … expressed the fear that the machine would react to the lack of angle of incidence in the wing by dropping its tail and would thus presumably be obliged to take off in an extremely unstable attitude. Unfortunately the sceptic in one proved to be right, for I hung in the air like a "pregnant duck" after take-off and could only rejoice when, after flying painfully down the airfield, I felt solid ground under my wheels again just short of the airfield at Aldershof. The second pilot had no greater success, not until the cat's back aerofoil was modified to give it an angle of incidence could we venture to fly a turn, but even now the pregnant duck had merely become a lame duck'.

Considering the basic definition of lift as the force created on an object at right angles to the incident flow, it is evident that such a force, like all forces according to Newton's Second Law, will be associated with a rate of change of momentum in that direction. Thus, the magnitude of the lift force will, in principle, be unambiguously determined by integrating all the components of momentum in the flow field normal to the incident flow that result from the object causing deviation of the flow.

Whilst this explanation is pure and fundamental, it does not immediately shed light on why lift forces can be so large.

The explanation relating to Bernoulli's equation has some relevance here. Where flow is accelerated around a curved surface, the reduction in static pressure assists in maintaining attachment of the flow and contributes to large suction forces. As nature proverbially abhors a vacuum, strong suction on the boundary layer near a curved surface will induce a large deviation in the general fluid flow some distance from the surface, thereby giving a large overall change in fluid momentum and producing a strong lift force. Aerofoil design is very much about the extent to which such forces can be sustained as the curvature is increased and more severe changes of flow direction are attempted in order to increase lift.

An associated consequence of the Bernoulli equation is the so-called Coanda effect. Aerofoils with elliptical section were developed and used on the X-wing plane/helicopter design [12]. Such aerofoils will have only moderate lifting capability attributable to their shape alone. However, the discharge of a thin jet of air tangential to the surface near the trailing edge will attract the general flow to the jet and cause a much larger deviation in flow direction and consequently much enhanced lift.

The 'attraction' of the jet to the surface arises as the jet brings increased momentum into the boundary layer where the jet flow is next to the body surface. This overcomes the natural tendency of the (reduced momentum) boundary layer to separate under the adverse (rising) streamwise pressure gradient due to the aerofoil curvature. Due to the large curvatures involved, there is a noticeable pressure change across the jet, which can be calculated from the mass flow rate in the jet and the radius of curvature of the flow. The jet tries to entrain any fluid between itself and the wall (very efficiently because it is normally turbulent) and this entrainment keeps it attached to the wall. Then, because the streamlines are now curved, the wall pressure falls below the external ambient value. In fact, in the absence of external flow incident on the aerofoil, such a jet will almost completely encircle the aerofoil.

This phenomenon is often called the Coanda effect in recognition of Henri-Marie Coanda, who discovered it apparently through rather hazardous personal experience.[2] Controlling lift on an aerofoil section by blowing a jet tangential to the surface is often referred to as circulation control. It is a form of boundary layer control which has been considered for regulation of loads and control or performance enhancement of wind turbine blades [13].

Lift is intimately related to vorticity [14]. Associated with this is the Magnus effect, whereby a rotating cylinder (or sphere) can generate lift. This affects the flight of balls in many sports, has been employed in the form of the Flettner rotor [15] to power ships and

2 Henri Coanda was asked to devise a system to divert the hot jet discharges from an aircraft's engines away from the cockpit and fuselage. In blowing air to this end, the jet did exactly the opposite and attracted the hot gases to the fuselage surface with dangerous consequences.

has been exploited in at least two innovative wind turbine designs [16, 17]. Wikipedia [18] is quite informative on lift, vorticity and the Magnus effect and also provides a commentary on some popular incomplete views such as have been discussed. Finally, in the context of wind turbine systems, lift may also be involved in the performance of wind devices that have been casually categorised as 'drag' devices (see Section 13.2).

1.3 Power in the Wind

In ideal modelling of wind flow, it is usual to start with a wind field that is of uniform constant velocity everywhere, introduce an energy extraction system such as a rotor and examine the resultant flow field that is established in steady state. For subsequent clarity, the basic conservation laws of a particle as compared with steady-state flow are recalled in Table 1.1. Generally, in discussion of steady-state flows, it has been common to use the particle-related terminology rather loosely (e.g. talking about momentum theories where it is really momentum rate or force that is being considered or energy balances that are really power).

Referring to an axisymmetric enclosed surface bounding the flow volume that is continually passing through the rotor disc as the bounding streamtube, power flowing through the far upstream area at the source of that streamtube comprises kinetic power and, most importantly, also pressure power. The fundamental expression for power in the air is illustrated in Figure 1.1. In the notation adopted, m, U_0, V, p, A and ρ are respectively mass, air velocity, volume, pressure, area and air density.

The expression for source power in the wind is widely disseminated as $0.5\rho U_0^3 A_0$. However, this is incomplete being only the kinetic power and has led to many misunderstandings,[3] especially in the context of systems that aim to exploit flow augmentation and also in analysis of the rotating wake. Any volume, V, of gas at pressure, p, stores an amount of energy $E = pV$, which becomes a power $P = p\dot{V} = pAU$, if there is steady

Table 1.1 Conservation laws.

Particle	Steady flow process	
Mass	Mass flow rate	
Energy	Energy rate	$\Longrightarrow$ Power
Linear momentum	Linear momentum rate	$\Longrightarrow$ Force
Angular momentum	Angular momentum rate	$\Longrightarrow$ Torque

3 The almost universal teaching that the power in the wind is proportional to the cube of velocity, without mention or inclusion of the pressure power, has led to terrible misunderstandings, especially with regard to systems that augment flow. The author is aware of a system (never actually manufactured) that enhanced flow by a factor of ∼1.2 (eventually verified by computational fluid dynamic (CFD) modelling) but was marketed via business plans based on the assumption of $(1.2)^3$ power augmentation as opposed to ∼1.2. This fundamental error was maintained in financial calculations with ownership of the technology changing hands over a period of ∼30 years.

Figure 1.1 Power in the air.

Total energy	$\equiv$	kinetic + potential	$= \frac{1}{2}mU_0^2 + pV$
Pressure	$\equiv$	energy/unit volume	$= \frac{1}{2}\rho U_0^2 + p$
Force	$\equiv$	pressure $\times$ area	$= \frac{1}{2}\rho U_0^2 A + pA$
Power	$\equiv$	force $\times$ velocity	$= \frac{1}{2}\rho A U_0^3 + pAU_0$

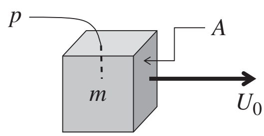

flow at velocity, U, through a surface area, A, of the volume, V. The correct expression for source power must therefore include both kinetic and pressure power and is:

$$\text{Source power in the wind, } P_0 = 0.5\rho U_0^3 A_0 + p_0 A_0 U_0 \tag{1.1}$$

The subscript, 0, denotes values far upstream prior to any energy extraction. The second equation of Figure 1.1 is Bernoulli's equation in the usual form for many wind energy analyses, where only energy associated with fluid pressure and velocity is considered. Clearly, there would be a fundamental inconsistency if the pressure-related term in the first equation of Figure 1.1 or in Equation 1.1 were missing. Relative to vacuum pressure, the pressure power term is huge,[4] but very small differences in it create the atmospheric wind resource and play a critical role in all wind power conversion systems. A quick perspective on the relevant pressure differences may be gained considering an extreme storm gust of $U = 70\,\text{m/s}$ which corresponds to a dynamic pressure of $0.5\rho U^2 \cong 3000\,\text{Pa} \cong 3\%$ of atmospheric pressure, while operation of any size of wind turbine at optimum aerodynamic performance in a wind of 10 m/s corresponds to a rotor plane pressure difference of <1% of atmospheric pressure. All forces on a wind turbine rotor and its capability to extract energy arise in consequence of such small pressure differences.

Further it must be emphasised, as appears in the discussion in Section 1.5.4, that kinetic energy is never directly extracted in any physical process. It is always converted to another form such as pressure energy or heat. All aerodynamic machines exploit pressure energy changes to provide the forces that do work.

1.4 The Actuator Disc Concept

The actuator disc is a valuable concept that arose early on in the development of analyses of rotors and propellers. Without any specific knowledge of or assumptions about

4 Otto Von Guericke's famous experiment of 1654 demonstrated that two teams of eight horses could not pull apart a large pair of touching copper hemispheres from which most of the air had been evacuated.

the system that may extract energy flowing through an arbitrary area in a uniform flow field, consideration of energy and momentum conservation allow some basic information about the consequent flow and limits on maximum possible energy extraction to be established.

A simple analysis of a rotor (or other energy extraction device) in open flow (Figure 1.2) leads to Froude's theorem[5] and the well-known Betz limit. In addition, actuator disc theory is further presented in a recently developed, more generalised form that will also deal with a rotor in *constrained* flow (Figure 1.3). Constrained flow is defined as the situation in which the following happens:

- An object is introduced into a flow field which modifies at least locally an otherwise uniform flow field of constant velocity.
- No energy is introduced or extracted by that object (conservative system).

An energy extraction device may then be introduced into the constrained flow field, in principle anywhere but most usually in a region of *flow concentration* where there is a higher local velocity and hence higher mass flow through unit area normal to the flow than in the far upstream flow. Typical examples of constrained flow are where there is a hill, a duct or a diffuser.

In the context of evaluating innovation, the point of considering this more general situation is twofold. Understanding the limitations on power performance of wind farms in complex terrain (hills) is a mainstream concern. Although there are no mainstream large-scale commercial wind energy systems that exploit flow concentration systems, nevertheless such systems have long been considered, some developed to prototype stage and others are under development at present. So they continue to receive increasing attention among innovative wind turbine designs.

Figure 1.2 represents a rotor in open flow. The flow field in the absence of the rotor would be of constant velocity everywhere and parallel to the axis of the rotor. Figure 1.3 represents a rotor in a diffuser (toroid with aerofoil cross section, as indicated). This is an example of constrained flow. Even in the absence of the rotor and of any energy extraction, the flow in a region around the diffuser is altered[6] by its presence and is substantially non-uniform.

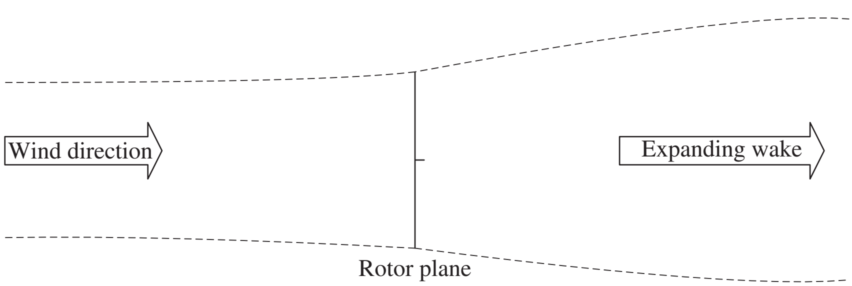

Figure 1.2 Open flow.

5 This is the result (for open flow) that the velocity at the rotor (energy extraction) plane is the average of the far upstream velocity and far wake velocity.

6 It may also be noted that the ground itself, even if completely level, constrains the flow. Although the ground effect extends in all directions to infinity, its constraint effect on the streamlines does exist locally near the wind turbine as if there is a mirror image of the turbine in the ground. It is not normally taken into account, but the effect is quite noticeable, for example, on the wake which because of its swirl lies at a small

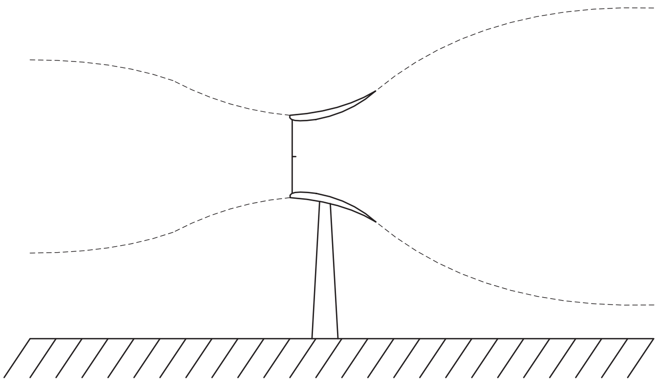

Figure 1.3 Constrained flow example (diffuser).

1.5 Open Flow Actuator Disc

1.5.1 Power Balance

The axial induction at the rotor plane is defined as the fractional reduction in far upstream wind speed local to the rotor. Thus (see Figure 1.4), the velocity through the rotor plane is;

$$U_1 = U_0(1 - a) \tag{1.2}$$

A key assumption in the actuator disc model of a wind turbine system (without wake rotation) that atmospheric pressure is restored in the far wake ($p_2 = p_0$). Conservation of mass in the steady-state process requires that there is the same constant mass flow rate $\rho A_0 U_0 = \rho A_1 U_1 = \rho A_2 U_2$ everywhere within the streamtube bounding the rotor plane. Thus, the pressure power, $p_0 A_0 U_0 = p_2 A_2 U_2$, is unchanged in the overall process, although it necessarily changes across the rotor plane (see Figure 1.6). Considering change in kinetic energy between far upstream and far wake, the power (rate of change

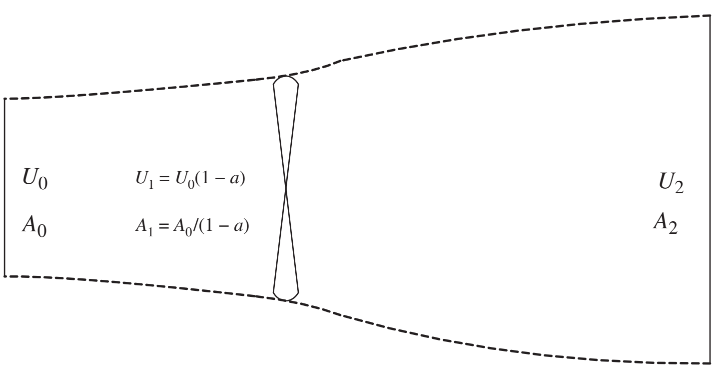

Figure 1.4 Open flow actuator disc model.

angle to the free stream. In contrast, the wind shear effect associated with the ground boundary layer is not due to the normal velocity constraint and extends everywhere independent of the presence of the turbine.

of kinetic energy) extracted P is

$$P = \frac{1}{2}\rho A_0 U_0^3 - \frac{1}{2}\rho A_2 U_2^3 \tag{1.3}$$

Since, $\rho A_0 U_0 = \rho A_2 U_2$:

$$P = \frac{1}{2}\rho A_0 U_0 (U_0^2 - U_2^2) \tag{1.4}$$

1.5.2 Axial Force Balance

The mass flow rate through the rotor plane is $\rho A_1 U_1$. The change in fluid velocity between upstream far wake is $(U_0 - U_2)$. Hence, rotor thrust as rate of change of momentum through the rotor plane is

$$T = \rho A_1 U_1 (U_0 - U_2) \tag{1.5}$$

and power, P is

$$P = TU_1 \tag{1.6}$$

$$= \rho A_0 U_0^2 (1 - a)(U_0 - U_2) \tag{1.7}$$

1.5.3 Froude's Theorem and the Betz Limit

From Equations 1.4 and 1.7

$$U_2 = U_0(1 - 2a) \tag{1.8}$$

It can be seen that the far wake induction is thus twice the value at the rotor plane. This result was first derived by Froude [19]. Defining power coefficient C_p as the ratio of fraction of power extracted by the rotor to the amount of kinetic power that would pass through the rotor swept area with the rotor absent, then:

$$P = \frac{1}{2}\rho\, A_1 U_0^3 C_p \tag{1.9}$$

Using Equation 1.8 to substitute for U_2 in Equation 1.7 and also noting that $A_0 = A_1(1 - a)$

$$C_p = 4a(1 - a)^2 \tag{1.10}$$

Differentiating Equation 1.10 to determine a maximum leads to $a = 1/3$ and to the Betz limit:

$$C_p = 16/27 \tag{1.11}$$

Investigations by Bergey [20] and van Kuik [21] indicated that Lanchester (1915), Betz (1920) and Joukowski (1920) suggested that all, probably independently and certainly by methods differing in detail, have determined the maximum efficiency of an energy extraction device in open flow. Later, Okulov and van Kuik [22] concluded that the attribution to Lanchester by Bergey was inappropriate. Thus, the Betz limit may apparently most properly be called the Betz–Joukowski limit, although for convenience the short reference as Betz limit is retained.

Although open flow actuator disc theory is over a century old, it is by no means done and dusted. The Betz limit and the ideal actuator disc have been the subject of extensive and continuing discussions. In real flow, external flow that does not pass through the rotor plane may assist in transport of the wake and therefore contribute additional energy to the system. However, this goes beyond the ideal actuator disc in inviscid flow, which cannot be expected to reflect behaviour at the tip of a real rotor with discrete blades or address gains and losses associated with viscous flow effects.

Although it is now confirmed both theoretically (in the following analysis, for example) and by numerical analyses based on vortex theory [23, 24], the validity of the Betz limit for ideal inviscid flow through an actuator disc had been questioned. Greet [25], considering a one-dimensional analysis, and Rauh and Seelert [26], considering 3D axisymmetric potential flow, arrived at the same conclusion that Froude's theorem and the Betz limit could not be rigorously be proved. They considered the problem to be a failure to account fully for streamtube forces. There were no analytical errors in their analyses, but they reached an impasse and formed false conclusions on failing to conduct a complete momentum balance considering external as well as internal forces on the streamtube. Energy extraction relates only to the magnitude of the streamtube areas far upstream, at the plane of the disc and far downstream, but the shape, pressure distribution and axial force on the streamtube boundary arises intrinsically from a balance of static pressure between internal and external flows. Thus, total streamtube forces will be indeterminate if an analysis does not consider a control volume as in Figure 1.5 that includes some external flow.

The streamtube is of course a virtual entity like a line or geometric figure. It has specific properties that no fluid and hence energy or momentum flows across its boundaries. However, for any chosen volume within a steady-state flow field, such as the volume, V, in Figure 1.5, it must be possible to demonstrate equilibrium of forces, mass flow, and so on. Otherwise, steady-state flow would not be maintained. The sum of axial streamtube forces is expressed by the integral over the whole surface enclosing the volume of the streamtube.

$$F_x = \oint p\widehat{dA}.\widehat{x} = p_0 A_0 - p_2 A_2 + \int_{A_0}^{A_2} pdA \tag{1.12}$$

In Equation 1.12, dA is an element of area normal to the axial direction with the vector direction of $\widehat{x}$, a unit vector in the axial direction. The integral is then split into end forces

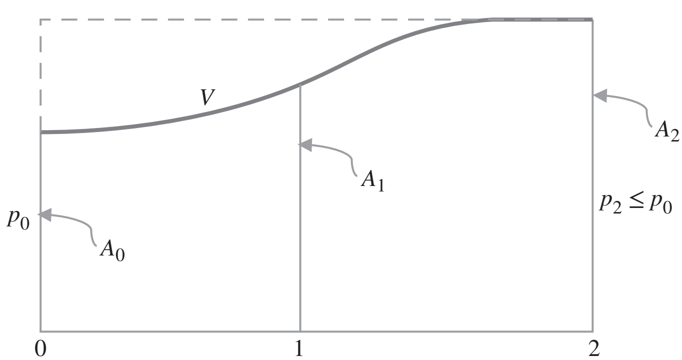

Figure 1.5 Axisymmetric control volumes for an actuator disc at plane 1.

at planes 0 (far upstream) and 2 (far downstream) plus the axial force on the curved surface. In the simple actuator disc model of Betz, the wake expands but is not rotating. The far downstream static pressure is then p_0, although the analysis presented considers the more general case where, if the wake is rotating, suction pressure is required to balance centrifugal force and hence the far downstream pressure, p_2, and indeed pressure anywhere inside the wake, will be less than p_0.

The momentum (axial force balance) equation for the ideal actuator disc, considered within the streamtube that bounds the disc, involves rate of change of fluid momentum, rotor plane thrust, T, and axial forces on the streamtube:

$$0 = \dot{m}(U_0 - U_2) - T + F_x \tag{1.13}$$

The sum of streamtube axial forces, F_x, is zero for the ideal actuator disc without wake rotation when $p_2 = p_0$. Sharpe [27] reasons that it can be deduced immediately observing that (in spite of local pressure variations on the curved surface) the whole streamtube that bounds the disc is ultimately immersed in fluid at atmospheric pressure. An explicit proof that $F_x = 0$ is now presented.

Consider the control volume, V, enclosed by the streamtube curved surfaces and the dotted lines. Mass flow enters axially through the annulus defined by the vertical dotted line and exits obliquely through the cylinder wall defined by the horizontal dotted line. Regarding the streamtube boundary as a 'wall', radial momentum is temporarily imparted to the flow (and later absorbed outside the control volume V when the streamtube curvature reverses). However, there is no energy extraction and hence no change in axial momentum of the external flow. Thus, the force associated with the fluid axial momentum rate at entry to the control volume, V, namely, $\rho(A_2 - A_0)U_0^2$, is exactly balanced by a similar term involving the integral of components of axial velocity over the exit area. The end force at plane 0 on the annulus represented by the vertical dotted line is then clearly $p_0\ (A_2 - A_0)$. There cannot be any axial force on the parallel surface. Thus, the curved surface axial force, F_c is given as:

$$F_c = \int_0^2 p dA = p_0\ (A_2 - A_0) \tag{1.14}$$

Considering Equation 1.12, this proves that $F_x = 0$ when $p_2 = p_0$ and so reduces Equation 1.13 to a balance of rate of change of fluid momentum with the thrust force as assumed by Betz.

1.5.4 The Power Extraction Process

The power balance for the ideal actuator disc is illustrated in Figure 1.6. A key assumption for the simplest case where the wake is not rotating is that general atmospheric pressure is recovered in the far wake so that $p_2 = p_0$. The actuator disc model requires continuity of the fluid axial velocity through the rotor plane. This is essential as the wind turbine removes energy from the air flow passing through it but does not remove any of the air itself! *Locally* at the rotor plane, with no change in axial velocity, there is no change in the associated kinetic power in the flow and *only pressure power is extracted*. Overall, considering source power far upstream and residual power far downstream, the assumption that the air pressure returns to ambient far downstream determines

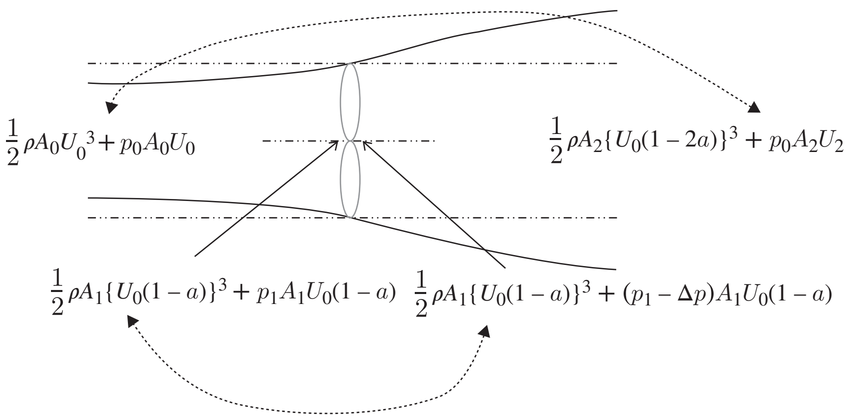

Figure 1.6 Power balance for ideal actuator disc (no wake rotation).

that there is no net change in pressure power ($p_2 = p_0$ and $A_2U_2 = A_0U_0$) and hence the overall process appears as an extraction of source kinetic power.

If locally the wind turbine rotor is not extracting kinetic energy and yet the system is producing power and therefore extracting energy from the fluid, what is the energy source? The answer is *potential energy*, which in this case is pressure energy. This is true of all fluid machines, fans, propellers, wind turbines and even gas turbines where thermal energy changes must be accounted but can only contribute to forces through creating or modifying pressure differences.

A wind turbine rotor produces power from the torque generated by the rotor blades. This torque arises from forces on blade elements, which in turn are the consequence of pressure differences on each side of the aerofoils. The wind turbine works by offering an appropriate resistance to the fluid flow slowing the fluid approaching the rotor. The reduction in fluid velocity occurs conservatively ahead of the rotor plane. Hence, considering Bernoulli's equation, a rise in static pressure occurs to provide conservation of energy per unit volume. The pressure difference across the rotor plane in conjunction with the through flow velocity is then the determinant of the energy extraction and, as was discussed previously, pressure is effectively potential energy per unit volume of fluid.

The basic equation for power at the rotor plane is then;

$$P = \Delta p\, A_1 U_1 \tag{1.15}$$

This defines power in the air flow through the actuator disc. Equation 1.15 is valid under all circumstances (open or augmented flow). Some of this power is not available to a rotary type of energy converter and remains in the air as the rotational kinetic power in the wake. In addition, some of the total power available to the rotor may not be converted usefully due to aerodynamic and drive train loss mechanisms.

1.5.5 Relativity in a Fluid Flow Field

According to basic physical laws established since the time of Galileo, who first described this principle in 1632 in his '*Dialogue Concerning the Two Chief World Systems*', velocity is relative and there is no preferred inertial frame. Thus, provided there is no significant interaction with a ground boundary layer, driving a rotor at

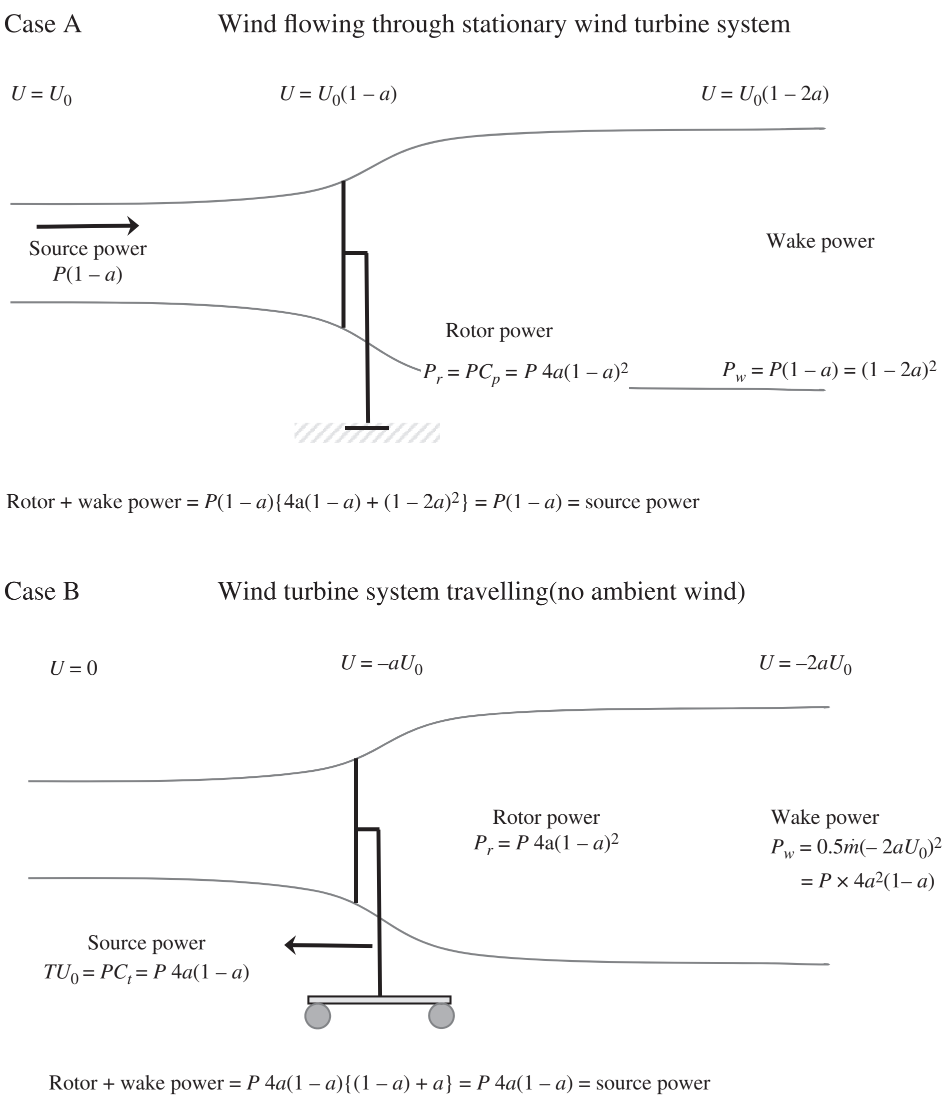

Figure 1.7 Power balance in reference frames of Cases A and B.

constant velocity U_0 through still air relative to a ground reference frame (Case A in Figure 1.7) must, *for the rotor*, be exactly equivalent to the rotor being mounted on a stationary support in a wind field of constant velocity U_0.

This has some practical significance. In a low wind region, it may take a long time to collect adequate data to characterise a power curve and driving a rotor through still air offers a valid, if not ideal, means of measuring rotor performance at least of small rotors. See Chapter 18 where this method is used in testing the Katru system. The analysis of this case shows that in different reference frames, velocities, momentum, energy and power measures change; but naturally energy and momentum are conserved and thus power also in a steady-state flow process. Also, with airborne systems (Chapter 8), it is often only in the reference frame of the moving airborne rotor that steady-state flow can be considered to exist and this may become a preferred frame for analysis.

Let $P = 0.5\rho\pi R^2 U_0^3$, where R is rotor radius. Let $.m$ be the mass flow rate of air in the streamtube bounding the rotor plane, as measured in the rest frame of the streamtube and wind turbine system.

Case A (Figure 1.7) is the normal situation where the wind turbine system is stationary relative to the ground and the upstream wind speed is U_0. In Case B (Figure 1.7), the upstream air is calm (no wind) and the wind turbine system is driven at speed U_0. If any effects related to ground proximity are ignored, then Galilean (also called Newtonian) relativity demands that the local velocity of air relative to the rotor plane is the same in each case, namely, $U_0(1 - a)$, that the physical process (power extracted by the rotor and shape of streamtube) is the same and that conservation laws are upheld.

There is superficially a paradox in that the work done by the rotor thrust, T, is $TU_0(1 - a)$ in Case A but TU_0 in Case B. This arises because the source power is different in each case. However, the rotor power is the same and energy conservation (power in steady-state flow) is satisfied as in both cases. The sum of rotor power and wake power is equal to source power.

1.6 Why a Rotor?

The actuator disc idea considers an arbitrary energy extraction system which need not be a rotor. Yet all present mainstream wind energy conversion systems rely on the rotor concept. Why? A wind energy system is not only, as is axiomatic, an energy conversion system turning fluid mechanical energy in the wind into electrical energy but is also an energy concentration system.

For example, a typical modern 1.5 MW wind turbine may have parameters as in Table 1.2. In a case when the wind turbine is producing its rated output (1500 kW in the generator output electrical cables) at 11.5 m/s rated wind speed, it has received wind energy over the swept area at a power density ~1 kW/m^2 and is transporting output after losses at a power density of around 1.6 GW/m^2. As the power passes through the system, it is concentrated first in the composite of the blades, then in the steel of the shaft, subsequently in the field of the generator and finally in the copper of the electrical cables.

It is vital to effect this massive concentration with as little cost as possible and the first major gain is made in the rotor itself. The rotor typically has a solidity of ~5% and hence blade frontal area is less than the swept area by a factor ~20. This is evident in the highlighted concentration factor (**19.1**, in Table 1.2).

This is the key factor in favour of the rotor concept. The rotor can confront all the extractable energy in the swept area with blades that may occupy only about 5% of the swept area. This is in direct contrast to a translating aerofoil or, say, an oscillatory wave energy device where, although the source energy density is usually much greater than for wind, a metre length of wave energy converter must confront each metre of wave front from which energy is to be extracted.

Thus, an efficient rotor is typically concentrating the extractable energy in the rotor disc by a factor of about 20 and thereby reducing the size and cost of the primary collectors (blades) compared with alternative systems such as an oscillating aerofoil that do not have this benefit. The answer to 'why a rotor?' is therefore not only the legitimate

Table 1.2 Power concentrations in a 1.5 MW wind turbine.

	D (m)	Area (m^2)	Efficiency	Power (kW)	Power density (kW/m^2)	Concentration factor	Cumulative concentration factor
Wind over swept area	70.5	3 900	1	3 640	0.93	1	1
Rotor blade input	70.5	204	0.44	3 640	17.83	**19.1**	19
Low speed shaft input	0.564	0.25	1	1 600	6 400	359.6	6 900
Gearbox input	0.564	0.25	0.98	1 600	6 280	1	6 900
Generator input	0.12	0.01	0.95	1 570	131 700	21.6	150 000
Electrical cables	—	0.001	1	1 490	1 490 000	10.7	1 600 000

common observation that mechanical energy in rotational form best suits conventional electricity generating systems but also that, in sweeping an area of the source energy flux that is much greater than the physical surface area of the rotor blades, the rotor effects a significant primary increase in energy density.

This is the main reason why the rotor concept is very hard to beat and why many of the alternatives such as oscillating or translating aerofoils that are perfectly feasible technically may struggle to be cost competitive.

1.7 Actuator Disc in Augmented Flow and Ducted Rotor Systems

1.7.1 Fundamentals

The ducted rotor system comprises a bare turbine rotor with an added surrounding structure intended to alter the inflow to the turbine in magnitude and or direction (diffusers and other types). It is commonplace in aeronautical and marine applications including ships and also tidal turbines.

The following statements are valid, but contrary views have been long standing.

a) The available (potentially extractable) power from any system with augmented flow (or not) is linearly proportional to the mass flow and to rotor plane pressure drop. In an augmented flow system, this is not as the cube of the velocity augmentation factor, although kinetic power through the rotor plane is augmented by this factor.
b) The maximum section diameter of a duct (exit area of a diffuser type) is a very obvious geometric parameter to consider, but *it has no unique relation to duct performance*. In particular, the view that ducted rotor performance is limited by the Betz limit as applied to the maximum duct diameter[7] is erroneous and misleading about the potential performance of ducts.

Regarding statement (a), ducted rotors in real flows may suffer adverse effects from friction losses and flow separation. However, they can also gain from viscous interaction

7 Sørensen [28] (pp. 22–23) provides an apparent derivation that Betz related to area ratio is a limit, but acknowledges that this relies on unverified assumptions.

with external flows. Thus, some energy that does not flow through the rotor may assist rotor performance by entraining the wake or in creating vortices that reduce pressure on the downstream side of the rotor plane. In some cases, essentially through increasing the pressure drop across the rotor (implying an ideal optimum $C_t > 8/9$), this can give a power gain that is somewhat better than linear with velocity augmentation. Such benefit has been observed in experimental testing by Phillips *et al.* [29] and Ohya and Karasudani [30], for example. In addition, much more elaborate systems can be developed to constructively involve the external flow involving boundary layer injection through slots, mixing and entrainment as developed by Werle and Presz [31] following practice in aircraft engine design.

Figure 1.8 shows three diffuser-type duct shapes among many more similarly analysed by McLaren–Gow [32] using a vortex ring model. Each duct has exactly the same area ratio (ratio of maximum to minimum duct diameter). The ducts were modelled as line ducts with no wall thickness and the C_p max for each design was determined by varying the rotor plane pressure drop. The inset table shows the ratio of (C_p max/1.161), the Betz limit factored by area ratio being $(16/27) \times (7/5)^2 = 1.161$. As an ideal inviscid analysis, this supports statement (b) showing that the area ratio is not a unique parameter. Evidently, the performance varies with duct shape and the performance is neither limited by nor related to the Betz limit as applied to the exit area. This refutes a common assertion that the ducted rotor can perform no better than a larger bare rotor with diameter equal to maximum duct diameter which, inappropriately, has led some parties to summarily dismiss ducted rotors as a concept. It will be shown (Chapter 18) that this is not simply the case for highly idealised inviscid flow conditions and that the limiting performance of some real systems probably exceeds the Betz limit as applied to the maximum duct diameter. While Figure 1.8 refutes the idea that Betz factored by area ratio is a valid limit, it is entirely consistent with the limit, 'C_p limit' in Figure 1.8, based on Equation 1.34. In the discussion around Equation 1.29, it is shown that C_p limit is in effect the Betz value applied to an area of streamtube section at a so-called reference plane. That area generally exceeds the maximum section area of the duct unless the duct is producing little augmentation and the wake does not expand beyond the duct exit. Seven duct shapes of the same exit area ratio (see later discussion of Figure 1.11) were analysed including the

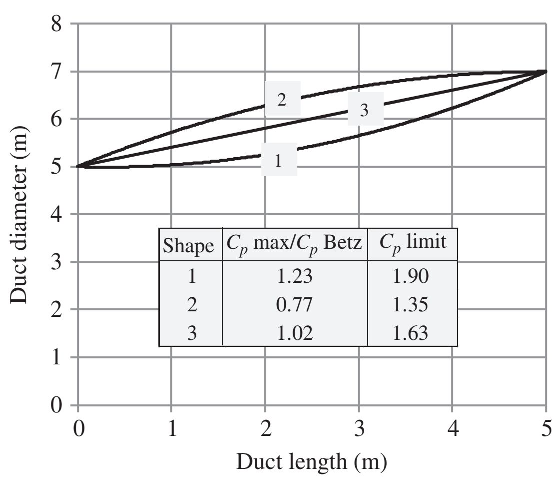

Shape	C_p max/C_p Betz	C_p limit
1	1.23	1.90
2	0.77	1.35
3	1.02	1.63

Figure 1.8 Area ratio fallacy.

three of Figure 1.8. Those that were of a more concave shape than duct 2 of Figure 1.8 (as viewed from the axis of symmetry) had a maximum ideal power coefficient less than Betz factored by the area ratio and those more convex than duct 1 exceeded Betz so factored. This is further clarified in Section 1.7.2. For any duct design where the flow expands downstream to an area greater than the exit area, the reference plane is also downstream of the duct, of greater diameter than the exit diameter and consequently defines a limit greater than Betz factored by area ratio.

In the early 1980s, Oman *et al.* [33] conducted experimental work on the diffuser-augmented wind turbine (DAWT) concept, showing that power coefficients exceeding the Betz limit could be obtained. In 1999, Hansen *et al.* [34] published CFD results confirming that the Betz limit could be exceeded. Hansen noted that the increase in C_p was in proportion to the augmentation of mass flow achieved by the diffuser (as in the discussion of Figure 1.13), but that this did not explicitly define a limit for C_p.

1.7.2 Generalised Actuator Disc

Although the open flow actuator disc theory, which determines the Betz limit, has evidently been established for over 90 years and van Bussel [35] in a comprehensive review notes that diffuser research has been in progress over 50 years, the generalisation of actuator disc theory arises from analysis by Jamieson [36]. This work includes new relationships for limiting values of C_p and a preliminary validation has shown close quantitative agreement with Hansen's CFD results [34]. In many previous analyses of turbines in ducts and diffusers, speedup factors are introduced and definitions of C_p and C_t other than the standard ones have been employed. This is understandable in the historical context, but there is no longer need for it and there is some potential for confusion. The following analysis maintains standard definitions of axial induction, power and thrust coefficients.

Axial induction, a, at the rotor plane is defined exactly as before (Equation 1.2). Thus, if the flow is augmented at the rotor plane, a is negative. As in open flow, the power coefficient and thrust coefficient are defined with respect to the far upstream wind speed and referenced to the rotor swept area. They are, respectively:

$$C_p = \frac{P}{\frac{1}{2}\rho A U_0^3} \tag{1.16}$$

and

$$C_t = \frac{T}{\frac{1}{2}\rho A U_0^2} \tag{1.17}$$

From these basic definitions of the power coefficient, C_p, and the thrust coefficient, C_t, the power to thrust ratio can be expressed as in Equation 1.18.

$$\frac{P}{T} = U_0 \frac{C_p}{C_t} \tag{1.18}$$

However, considering also the basic definition of power as a product of force and velocity as applied at the rotor plane:

$$P = T\,U_0(1 - a) \tag{1.19}$$

Hence,

$$\frac{P}{T} = U_0(1 - a) \tag{1.20}$$

Hence, from Equations 1.18 and 1.20,

$$\frac{C_p}{C_t} = (1 - a) \tag{1.21}$$

Equation 1.21 applies to an ideal rotor in open or augmented flow, where the local inflow is a fraction $(1 - a)$ of the remote undisturbed external wind speed. A system is defined as the region in which axial induction is influenced between the freestream and the far wake. Energy extraction is considered to take place across a planar area normal to the flow and at a definite location within the system.

Let $f(a)$ be the axial induction in the far wake (Figure 1.9). At any plane of area, A within the system where there is a pressure difference, Δp associated with energy extraction, the thrust, T is given as;

$$T = \Delta pA = \frac{1}{2}\rho U_0^2 A C_t \tag{1.22}$$

Hence

$$C_t = \frac{2\Delta p}{\rho U_0^2} \tag{1.23}$$

Considering Bernoulli's equation, applied upwind of the extraction plane,

$$p_0 + \frac{1}{2}\rho U_0^2 = p_1 + \frac{1}{2}\rho U_0^2 (1 - a)^2 \tag{1.24}$$

and on the downstream side of the extraction plane.

$$p_1 - \Delta p + \frac{1}{2}\rho U_0^2 (1 - a)^2 = p_0 + \frac{1}{2}\rho U_0^2 \{1 - f(a)\}^2 \tag{1.25}$$

From Equations 1.23–1.25,

$$C_t = 1 - \{1 - f(a)\}^2 \tag{1.26}$$

$$C_t = 2f(a) - f(a)^2 \tag{1.27}$$

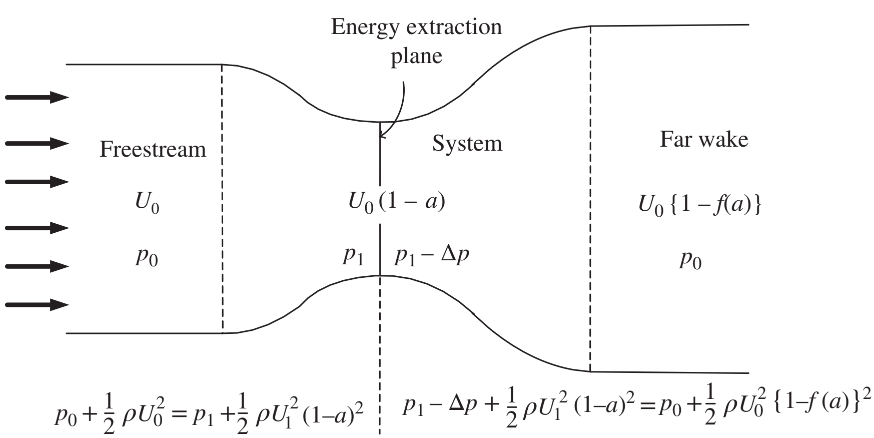

Figure 1.9 General flow diagram.

Now consider that:

a) For energy extraction to take place, the velocity in the far wake must be less than ambient, that is, $f(a) > 0$
b) If the flow is augmented above ambient at the rotor plane, then purely from considerations of continuity, there must exist a reference plane of area A_{ref} downstream of the rotor plane where the induction is half that of the far wake, that is, $= f(a)/2$

Considering conservation of mass in the flow, then at the rotor plane (area A_r),

$$\rho A_r U_0(1 - a) = \rho A_{\text{ref}} U_0 \left(1 - \frac{f(a)}{2}\right) \tag{1.28}$$

The factor of 2 in Equation 1.28 may initially seem arbitrary. However, the idea is to view the augmentation system as a disturbance ahead of the reference plane, which itself is in open flow at a location where Froude's theorem and the established formulae for C_t and C_p can apply if related to the axial induction there. Now for Froude's theorem to apply, the induction is required to be specifically 1/2 of $f(a)$ as distinct from any other fraction. This also implies that *the Betz limit applied to the reference plane area* (as opposed to the duct maximum diameter) must be the valid ideal inviscid performance limit for the duct under consideration. In the absence of energy extraction, note that $f(a) = 0$.

Let the axial induction at the energy extraction plane be a_0. Then,

$$\rho A_r U_0(1 - a_0) = \rho A_{\text{ref}} U_0 \tag{1.29}$$

In Figure 1.10, streamtube sections bounding the diffuser are illustrated for differing levels of rotor disc pressure drop. From Equation 1.29, the reference plane has invariant area $A_r(1 - a_0)$ and 'moves' from far downstream at zero disc loading towards the rotor plane as disc loading is increased.

Seven duct shapes, as in Figure 1.11, were analysed as axisymmetric line ducts by MacLaren–Gow *et al.* [32] using a vortex ring model (three of these appear in Figure 1.8).

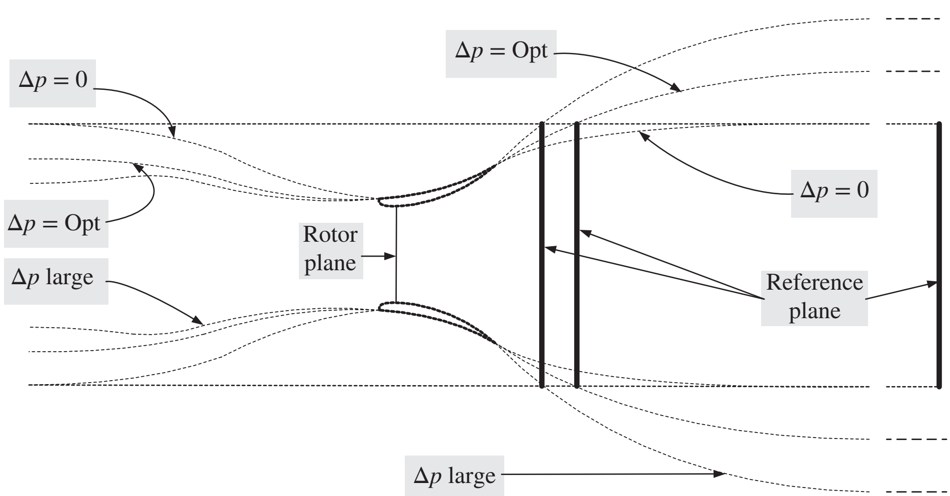

Figure 1.10 The reference plane in relation to disc loading.

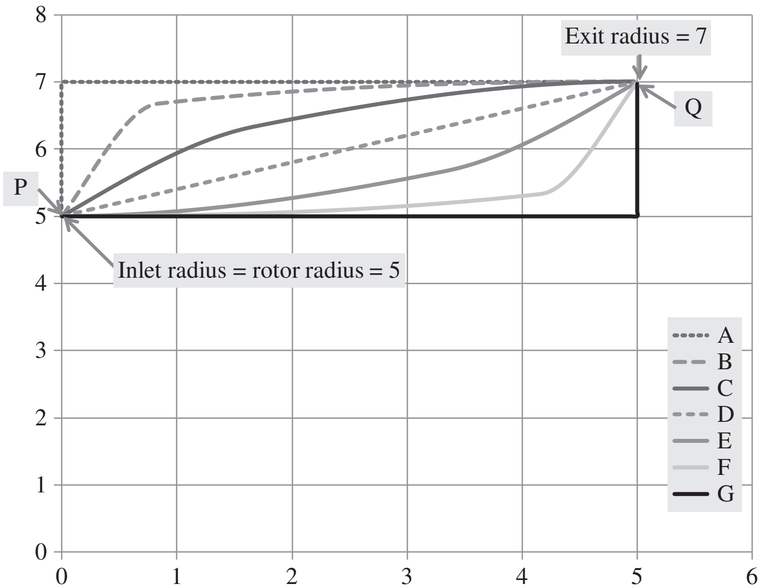

Figure 1.11 Seven shapes of line duct analysed as in inviscid flow.

Table 1.3 Limiting performance of ducts.

	A	B	C	D	E	F	G
Reference plane radius	6.116	6.204	6.383	7.187	8.033	8.778	9.433
C_p/Betz at reference plane	0.922	0.931	0.943	0.968	0.977	0.977	0.970
C_p/Betz at exit plane	0.707	0.734	0.787	1.025	1.292	1.542	1.768

The inlet radius (also the rotor plane radius) is always 5 units and the exit 7 units. As C_p increases from poorest duct A, to best G, the reference plane moves downstream from within the duct (with radius less than exit radius of 7 units) to values substantially exceeding the exit radius. In other words, flow expansion takes place beyond the duct exit.

The C_p values at the reference plane (Table 1.3) are all close to the Betz limit by amounts that can be related to C_t at maximum C_p. The C_p performance can, moreover, be seen to be quite unrelated to exit area ratio with values ranging from 29% less to 77% greater.

Returning to Figure 1.10, a detail reflects behaviour also observed in numerical modelling. Especially with higher loading on the disc, the inflow streamtubes, 'sensing' flow resistance ahead, start to expand (see 'Δp large' in Figure 1.10) as would happen for an open flow rotor before they contract due to the suction of the diffuser.

From Equations 1.28 and 1.29,

$$f(a) = 2\left\{\frac{a - a_0}{1 - a_0}\right\} \tag{1.30}$$

Now substituting for $f(a)$ in Equation 1.27, gives

$$C_t = \frac{4(a - a_0)(1 - a)}{(1 - a_0)^2} \tag{1.31}$$

And hence from Equation 1.21:

$$C_p = \frac{4(a - a_0)(1 - a)^2}{(1 - a_0)^2} \tag{1.32}$$

Differentiating Equation 1.32 with respect to a determines a maximum at $a = a_m$ of

$$a_m = \frac{1 + 2a_0}{3} \tag{1.33}$$

The associated maximum C_p is then:

$$C_{pm} = \frac{16}{27}(1 - a_0) \tag{1.34}$$

For the open flow rotor with $a_0 = 0$, Equations 1.31–1.34 correspond, as they must, to the established equations for open flow. The familiar results that the open flow rotor operates optimally when $a_m = 1/3$ and has an associated maximum power coefficient $C_{pm} = 16/27$ (the Betz limit) are evident.

A more striking result emerges out of the limit Equation 1.32. On substituting a_m from Equation 1.33 in Equation 1.32, it is found that

$$C_t = \frac{8}{9} \tag{1.35}$$

whereas a_m and C_{pm} have specific values for each system configuration, this result is now independent of a_0. Equation 1.35 is therefore a general truth for optimum energy extraction in an ideal system. This result was mentioned to the author in 1995 by K. Foreman, as an observed outcome (without theoretical explanation) of his extensive experimental work within Grumman Aerospace in the 1980s with the DAWT concept. It was proved more recently by van Bussel [35] and now directly as a consequence of the generalised limit Equations 1.31 and 1.33. Considering Equation 1.23, a corollary to Equation 1.35 is that the pressure drop across the rotor plane for optimum energy extraction is always $4/9U_0^2$.

Thus, in any flow field of uniform far upstream velocity, U_0, *regardless of what local flow augmentations are created (conservatively) within the system and wherever a rotor is located,* the rotor will, in optimum operation to maximise power extraction, experience the same loading in terms of thrust, T, thrust coefficient C_t and rotor plane pressure drop Δp. This does not in the least contradict statements in many sources (e.g. Lawn [37]) that a rotor in augmented flow must be 'lightly loaded'. Loading it at the same level of thrust as would be optimum in open flow, when the wind speed local to the rotor may be several times greater than ambient, amounts to very 'light' loading. The level of loading is independent of the level of flow augmentation achieved by the diffuser and will therefore appear all the lighter, the greater the flow augmentation.

Results are summarised in Table 1.4. Consider now Figure 1.12 where, instead of fixing the rotor swept area, the source flow area is fixed. With the same source flow area, the source mass flow rate and source power are the same in all three cases, namely, the general case with an arbitrary system, the particular case of a diffuser concentrator and the standard case in open flow.

Table 1.4 Summary results comparing open and constrained flow.

	Betz open flow	**Generalised constrained flow**
General operation		
Upstream wind speed	U_0	U_0
Wind speed at energy extraction plane	$U_0(1-a)$	$U_0(1-a)$
Far wake wind speed	$U_0(1-2a)$	$U_0\left(\dfrac{1-2a+a_0}{1-a_0}\right)$
Performance coefficient, C_p	$4a(1-a)^2$	$\dfrac{4(a-a_0)(1-a)^2}{(1-a_0)^2}$
Thrust coefficient, C_T	$4a(1-a)$	$\dfrac{4(a-a_0)(1-a)}{(1-a_0)^2}$
Pressure difference across rotor	$\frac{1}{2}\rho U_0^2 C_T$	$\frac{1}{2}\rho U_0^2 C_T$
Optimum performance		
Maximum C_p	$\dfrac{16}{27}$	$\dfrac{16}{27}(1-a_0)$
Associated axial induction factor	$\dfrac{1}{3}$	$\dfrac{1+2a_0}{3}$
Far wake axial induction factor	$\dfrac{2}{3}$	$\dfrac{2}{3}$
Associated thrust coefficient	$\dfrac{8}{9}$	$\dfrac{8}{9}$
Pressure difference across rotor	$\frac{4}{9}\rho U_0^2$	$\frac{4}{9}\rho U_0^2$

From Equation 1.34

$$C_{pm} = \frac{16}{27}(1-a_0)$$

Energy extracted by the rotor is, by definition:

$$E_1 = \frac{1}{2}\rho U_0^3 A_1 C_{pm}$$

From continuity of flow;

$$E_1 = \frac{1}{2}\rho U_0^3 \frac{A_0}{(1-a_m)} C_{pm}$$

Using Equation 1.35

$$E_1 = \frac{1}{2}\rho U_0^3 A_0 \frac{8}{9}$$

The power available to the rotor evidently is 8/9 of the kinetic power in the upstream source area. Note that the thrust coefficient is identically equal to the fraction of source kinetic power that is extracted. Note also that all of the preceding analyses relate to

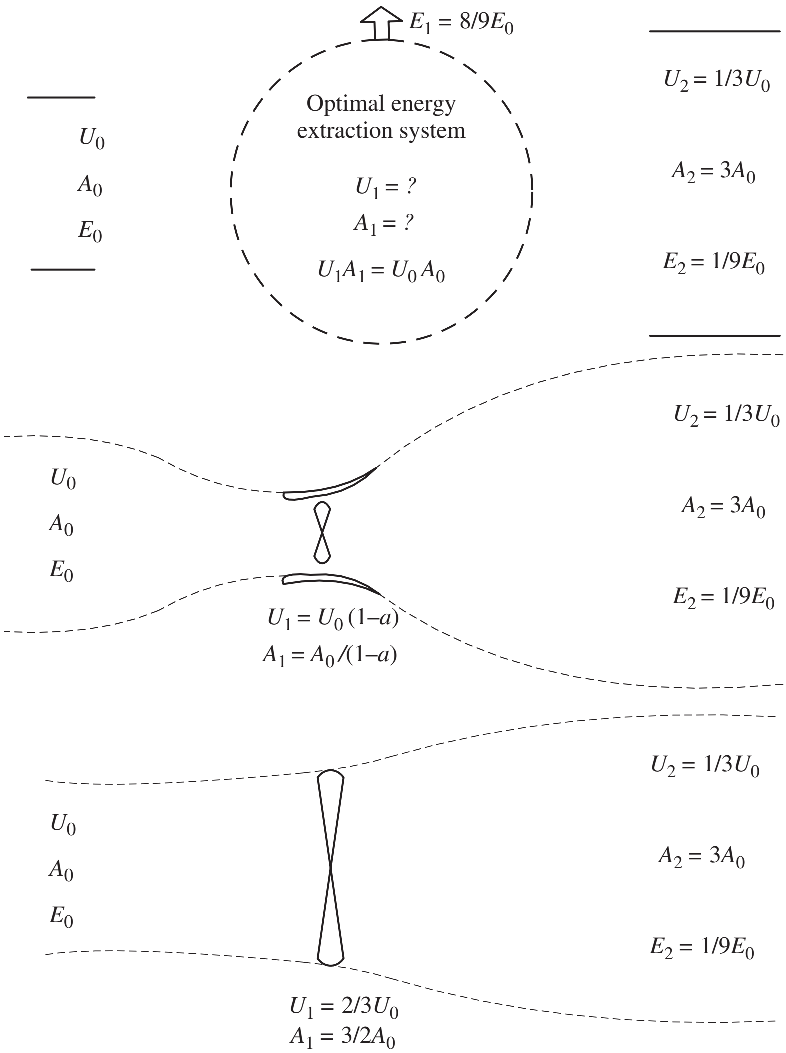

Figure 1.12 Comparison of cases with equal source flow areas.

ideal actuator discs as power extraction systems. This means that the wake does not rotate as it would with any real rotor system and that the assumption of wake pressure recovery to atmospheric pressure is valid. Wake rotation can, however, be extremely important for the aerodynamic performance of ducts in real flows. With a high tangential velocity component in the wake flow, the angle to horizontal of the resultant flow on its expanding spiral path is much less than the geometric expansion of the duct in the axial direction. This enables short ducts with high geometric expansion angles to perform effectively without premature flow separation.

In the open flow case, the 'system' is always 'ideal' in that the flow is unconstrained and free to flow through or around the rotor in a way that can vary with rotor loading. In all other cases, the system comprises some physical entity additional to the rotor which constrains the flow. In general, this system, whether hill, diffuser or other, because it is of fixed geometry, will not be ideal in every flow state and may not be ideal in any. Hence, even in terms of purely inviscid flow modelling, such systems, regardless of the efficiency of the rotor or energy extraction device, may not extract energy as efficiently as in open flow. Comparing an effective diffuser system with an open flow rotor that optimally extracts the same amount of energy, the rotor in the diffuser system can be much smaller in diameter and the critical design issue is whether this advantage can justify the cost of the diffuser system.

In the limit state (ideal device in ideal system):

- The design of the device is completely decoupled from design of the system, which is completely characterised by a_0.
- The thrust and thrust coefficient that corresponds to optimum rotor loading are independent of the system that includes the rotor and the thrust coefficient is always 8/9.

The conclusion from this is that for any system influencing the local flow through an energy extraction device, the induction factor, a_0, at the extraction plane with the device absent provides a characteristic signature of the system. This statement is probably valid for non-ideal energy extraction devices such as rotors with drag loss, tip loss and swirl loss provided the system influencing the rotor plane induction is ideal.

Consider now the operation of a rotor in constrained flow. The Internet is littered with websites where claims are made that some innovative system around a wind turbine increases the air velocity locally by a factor k and therefore the power as k^3.

In any area of flow augmentation prior to energy extraction, the flow concentrator does not introduce extra energy into the flow field. Therefore, increased local velocity and the associated increase in local kinetic energy are created conservatively. Hence, according to Bernoulli's theorem, increased kinetic energy is obtained at the expense of static pressure (atmospheric potential energy). It is perfectly true that the kinetic energy locally is increased by a factor k^3. This must be the case by definition. However, as has been strongly emphasised in Section 1.3, there is no extraction of kinetic energy at the rotor plane. It is the pressure difference at the rotor plane that drives energy extraction, and both the inlet and exit pressure of an energy extraction device in a region of concentrated flow are at sub-atmospheric pressure. This means that much less energy can be extracted than might be supposed.

Perhaps the simplest way to appreciate this is as follows. Consider a fixed area, A_0, represented by the dotted lines of Figure 1.13, where a rotor may be placed, but for the present in the absence of energy extraction. If the velocity is increased over the prevailing upstream value, U_0, by a factor, say, 3 in a flow augmentation device, the streamtube passing through it, by conservation of mass flow, will have an upstream source area that is three times greater than the extraction area, A_0. It is then clear that no more than three times the energy and certainly not 3^3 times can be extracted from this streamtube.

In Equation 1.15, $U_1 = U_0\,(1 - a)$ as defined in Equation 1.2. If the rotor is in a concentrator, a will be negative of a magnitude related to the flow augmentation factor, k (which, it should be noted, will change with rotor loading). Noting the results of Table 1.1, it can be seen that, for maximum energy extraction, in open flow or constrained flow, Equation 1.15 is unchanged. Hence, the increase in power is only linearly as the increase in local velocity in the region of flow concentration.

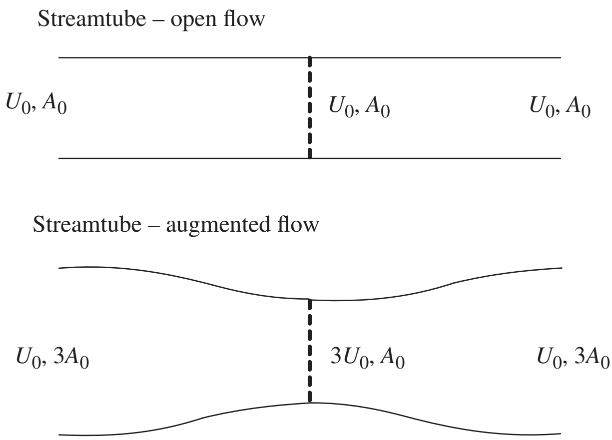

Figure 1.13 Source area and energy gain with flow augmentation.

The generalised actuator disc theory implies that all rotors whether large or small, whether in open flow or in well-optimised diffusers or other concentrators will operate optimally in an optimal system with a similar pressure difference across the rotor plane. This pressure difference under such ideal circumstances is $4/9\rho U_0^2$ (see Table 1.1). However, in constrained flow fields, system inefficiencies (which importantly can arise from purely geometric aspects in addition to frictional losses) will, in general, further reduce the optimal pressure difference for maximum energy extraction.

1.7.3 The Force on a Diffuser

From Equation 1.28, the mass flow rate through the energy extraction plane (and elsewhere) is $\rho A_r U_0(1-a)$; and from Equation 1.30, the change in fluid velocity between far upstream and far downstream is $f(a) = 2(a-a_0)/(1-a_0)$. Hence, the rate of change of momentum and total thrust force on the system is the product of these quantities.

$$T_{\text{net}} = \rho A_r U_0(1-a)\left\{\frac{2U_0(a-a_0)}{(1-a_0)}\right\} = \frac{1}{2}\rho A_r\, U_0^2\left\{\frac{4(1-a)(a-a_0)}{(1-a_0)}\right\} \tag{1.36}$$

Now, thrust on the rotor is, by definition:

$$T = \frac{1}{2}\rho A_r U_0^2 C_t$$

And hence from Equation 1.31:

$$T = \frac{1}{2}\rho A_r U_0^2\left\{\frac{4(1-a)(a-a_0)}{(1-a_0)^2}\right\} \tag{1.37}$$

Comparing Equations 1.36 and 1.37 it is clear that the force on the diffuser is,

$$T_d = \frac{1}{2}\rho A_r U_0^2\left\{\frac{-4a_0(1-a)(a-a_0)}{(1-a_0)^2}\right\} = -a_0 T \tag{1.38}$$

This very simple result is important. The separation of total system thrust into the part that acts on the rotor or energy extraction device and the part that acts on the diffuser or flow concentrator is vital for an appropriate implementation of BEM theory to deal with modelling of system loads or optimisation of rotors in constrained flows. Note also that, as far as inviscid flow is concerned, although thrust on the diffuser may be several times that on the rotor, thrust on the diffuser only appears in association with rotor loading and is zero on the empty duct.

The simple form of Equation 1.38 provides insight, but applies only to an ideal diffuser. Sørensen [28] asserts, '*In most theoretical analyses, the authors have introduced different auxiliary variables, in order to derive general conclusions concerning maximum power output, etc. However this is not necessary*…'. His implication is that the variable a_0 is unnecessary. However, he instead introduces the auxiliary variable, which he calls T_{diff} the force of the diffuser. Equation 1.38 shows clearly that a_0 is related and not additional to $T_{\mathrm{diff}} \equiv T_d$. The issue is simply that the level of augmentation and limiting performance of a diffuser differs, in general, for each possible diffuser geometry, and the limiting performance cannot be specified without introducing at least one integrated property of the diffuser. The introduction of a_0, in fact, provides a number of additional insights, among them relating velocity induction to duct force as in Equation 1.38.

Considering the diffuser as an axisymmetric aerofoil body, suction on the leading edge may, in general, produce a thrust component that is directed into the wind. The net force on the diffuser is then the sum of suction forces and pressure drag forces. When the diffuser is not ideal, the ratio of net force on diffuser to force on the rotor is increased and exceeds the prediction of Equation 1.38.

1.7.4 Generalised Actuator Disc Theory and Realistic Diffuser Design

The analysis presented here of ducts or diffusers in inviscid flow is only the starting point. Referring to this approach, which extends the open flow actuator disc theory to deal with augmented flows as 'generalised actuator disc (AD) theory', note that it

1) is a limiting theory (as is the Betz theory in open flow) that considers only inviscid flow,
2) shows clearly why flow concentration devices increase available energy linearly as increase of mass flow and not as the cube of the augmented velocity,
3) describes ideal systems, whereas real diffusers may be far from the limiting performance suggested; in general, their fixed geometry will only best suit one state of loading,
4) as an inviscid model, does not capture effects of flows external to the diffuser and rotor which can be used to augment performance through viscous interactions. Some diffusers are very much designed to exploit such effects as in the FloDesign wind turbine [38].

Generalised AD theory affords some new insights and provides energy limits for ideal systems, but there is still quite a gap between such ideal limiting theory and real-world design of flow augmentation systems.

The induction, a_0, of the ideal empty duct to be associated with a particular real duct can only crudely be estimated Jamieson [39] as $a_e \eta$ where a_e is the induction of the empty duct and η is the ratio of C_t associated with C_p max to 8/9. Moreover, determination of these parameters relies on detailed modelling of specific ducts. However, the generalised AD model refutes some fallacies about duct performance and does give a

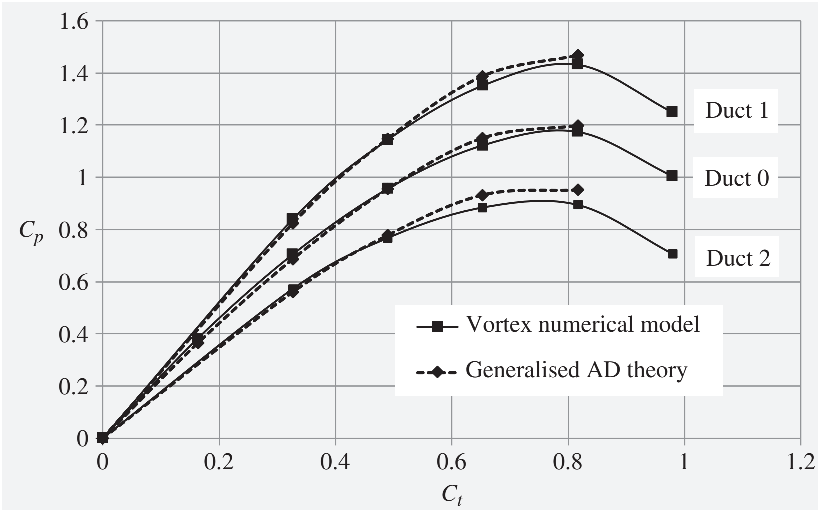

Figure 1.14 Performance characteristics of ducts.

reasonably self-consistent view of duct designs in inviscid flow (Figure 1.14) with some insights that are transferable to real duct design (Chapter 18). In Figure 1.14, results from the vortex ring model of McLaren–Gow [32] are compared with the generalised AD model based on Equation 23 of Jamieson [39].

1.8 Blade Element Momentum Theory

1.8.1 Introduction

BEM theory is the most widely used theory in practical design methods and computer codes for predicting loads and performance of wind turbines. In any balanced overview of wind turbine modelling reflecting current research directions, much attention would be devoted to vortex theories and CFD. These and numerical methods, in general, are not discussed. They may offer more accurate analysis of specific configurations, but they do not yield analytical relationships that can provide physical insight to guide parametric evaluations and concept design.

In BEM, the swept area of the rotor is considered as a set of annular areas (Figure 1.15) swept by each blade element. The blade is divided spanwise into a set of elements which are assumed to be independent of each other, so that balance of rate of change of fluid momentum with blade element forces can be separately established for each annular area. The basic theory is from Glauert [40], with the modern forms for numerical implementation in BEM codes having developed following the adaptation of Glauert's theory by Wilson *et al.* [41]. BEM theory is summarised here in order to preserve a self-contained account of some new equations that are developed from it.

1.8.2 Momentum Equations

Considering thrust as rate of change of linear momentum of the flow (overall axial velocity change, $2aU$ × mass flow rate) passing through an annulus at radius r of width dr and

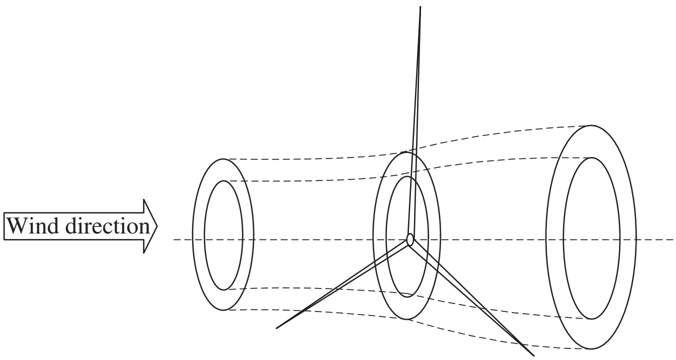

Figure 1.15 Actuator annulus.

denoting a tip effect factor (to be discussed) as F,

$$\text{Thrust} \quad dT = 4\pi\rho r U^2 a(1-a)F\,dr \tag{1.39}$$

and similarly considering torque and rate of change of angular momentum:

$$\text{Torque} \quad dQ = 4\pi\rho r^3 U a'\omega(1-a)F\,dr \tag{1.40}$$

In Equation 1.40, the tangential induction factor, $\acute{a}$ is introduced. The development of tangential velocity in the air occurs at the rotor plane and is considered to be from zero as the air is non-rotating immediately upstream of the rotor rising immediately downstream to a value of $2\acute{a}\omega$, which is the rotational angular velocity imparted to the wake by the torque reaction on the rotor. The torque reaction on the air grows from zero to maximum across the rotor plane and an average value of induction, $\acute{a}$, rather than $2\acute{a}$, is used in the flow triangle (Figure 1.16).

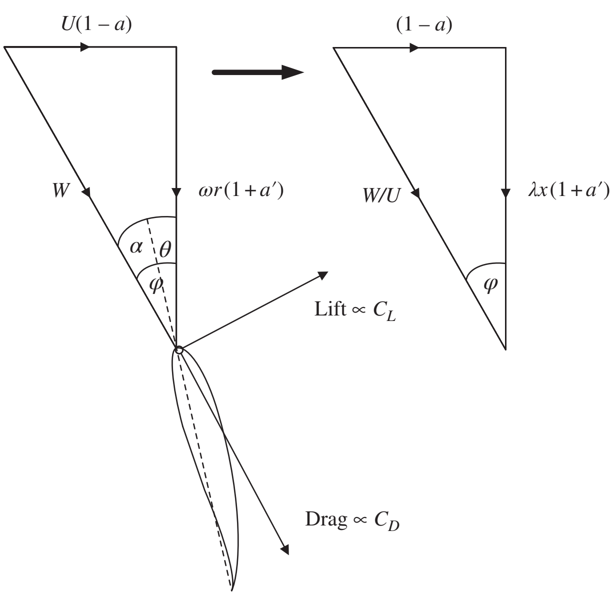

Figure 1.16 Local flow geometry at a blade element.

1.8.3 Blade Element Equations

Considering blade element forces on a blade element at radius r of width dr,

$$\text{Thrust} \quad dT = \frac{1}{2}\rho W^2 Bc(C_l \cos\varphi + C_D \sin\varphi)dr \tag{1.41}$$

$$\text{Torque} \quad dQ = \frac{1}{2}\rho W^2 Bc(C_L \sin\varphi - C_D \cos\varphi)rdr \tag{1.42}$$

Equations 1.39–1.42 allow dT and dQ to be eliminated, yielding two equations in the three unknowns, a, a' and φ. A third equation is given by considering the flow geometry local to each blade element at radius, r, that is at radius fraction, $x = r/R$.

From the flow geometry (Figure 1.16),

$$\tan\phi = \frac{U(1-a)}{\omega r(1+a')} = \frac{(1-a)}{\lambda x(1+a')} \tag{1.43}$$

Equating Equation 1.39 with Equation 1.41 and Equation 1.40 with Equation 1.42 to solve for the induced velocities a and a' (also making use of Equation 1.43) gives

$$\frac{a}{1-a} = \frac{\sigma(C_L + C_D \tan\varphi)}{4F\tan\varphi\sin\varphi} \tag{1.44}$$

$$\frac{a'}{1+a'} = \frac{\sigma(C_L \tan\varphi - C_D)}{4F\sin\varphi} \tag{1.45}$$

where σ, the local solidity, is defined as $\sigma = Bc/2\pi r$.

Usually, an iterative procedure is used to solve Equations 1.43–1.45 for each local blade element of width Δr. Hence, using Equations 1.41 and 1.42, the thrust and torque can be found on the whole rotor by integration.

The BEM analysis of Equations 1.39–1.45 has followed the widely used formulation of Wilson *et al.* [41], who suggested that drag should be neglected in determining the induction factors, a and a'. According to the PhD thesis of Walker [42]:

> … it has been the assumption that the drag terms should be omitted in calculations of a and a'… on the basis that the retarded air due to drag is confined to thin helical sheets in the wake and (will) have negligible effect on these factors.

Although drag must be accounted for in determining the torque and power developed by a rotor, opinion is divided[8] about whether the drag terms should be included in evaluation of the induction factors. Neglecting drag leads to simpler forms for Equations 1.44 and 1.45 and can enable a closed-form solution (Section 1.8.7). It also simplifies the following analyses.

1.8.4 Non-dimensional Lift Distribution

From Equation 1.43,

$$\frac{a}{1-a} = \left(\frac{Bc}{2\pi r}\right)\frac{C_L\cos\varphi + C_D\sin\varphi}{4F\sin^2\varphi} \tag{1.46}$$

$$= \frac{B}{8\pi}\left(\frac{cC_L}{R}\right)\left(\frac{R}{r}\right)\frac{(\cos\varphi + C_D/C_L\sin\varphi)}{F\sin^2\varphi} \tag{1.47}$$

---

8 DNV GL use the formulation including drag as presented in Equations 1.44 and 1.45 in their commercial BEM code, Bladed.

The term (cC_L/R) represents a non-dimensional lift distribution where the chord distribution $c \equiv c(\lambda, x)$ is, in general, a function of radius fraction, $x = r/R$, and design tip speed ratio, λ.

Let $\Lambda(\lambda, x) = \frac{c(\lambda,x)C_L}{R}$, and let $k = \frac{C_L}{C_D}$:

Then

$$\frac{a}{1-a} = \frac{\Lambda B}{8\pi x F}\frac{[1+(1/k)\tan\varphi]}{\sin\varphi\tan\varphi} \tag{1.48}$$

And

$$\sin\varphi = \frac{(1-a)}{\sqrt{(1-a)^2+\lambda^2x^2(1+a')^2}} \tag{1.49}$$

Hence, after some manipulation:

$$\Lambda(\lambda, x) = \frac{8\pi a(1-a)}{B\lambda(1+a')\sqrt{(1-a)^2+\lambda^2x^2(1+a')^2}}\frac{F}{\left[1+\dfrac{(1-a)}{k\lambda x(1+a')}\right]} \tag{1.50}$$

The tangential induction factor, a', can be solved as in Equation 1.51 in terms of a using Equations 1.43–1.45 to eliminate φ.

$$a' = \frac{\{\lambda^2k^2x^2+2\lambda kx-4ak[\lambda x-k(1-a)]+1\}^{0.5}-(\lambda kx+1)}{2\lambda kx} \tag{1.51}$$

Note that the elimination of φ in Equations 1.50 and 1.51 is only apparent as the lift-to-drag ratio, k, depends in general on the angle of attack, α, and $\alpha = \varphi(x) - \theta(x) - \psi$ where $\theta(x)$ is the blade twist distribution and ψ is the pitch angle of the blade. In the limit of zero drag when $k \to \infty$:

$$a' = \frac{(4a-4a^2+\lambda^2x^2)^{0.5}-\lambda x}{2\lambda x} \tag{1.52}$$

Equation 1.52 also appears in Manwell *et al.* [43].

With further approximation:

$$a' = \frac{a(1-a)}{\lambda^2x^2} \tag{1.53}$$

1.8.5 General Momentum Theory

When a rotating wake is considered in ideal inviscid flow, the angular momentum imparted to the air by torque reaction at the rotor plane is conserved and wake rotation is preserved through the whole of the wake. To balance the external pressure, the internal static pressure on the streamtube boundary of the far wake must be atmospheric. However, in order to maintain wake rotation by balancing centrifugal forces, the static pressure within the wake must reduce below ambient atmospheric. The power balance diagram is then similar to Figure 1.6; except that in the far wake, for any single stream tube annulus or for the average over the whole disc, the residual pressure power is now $p_2A_2U_2 = p_2A_0U_0$ where $p_2 < p_0$. Hence, unlike the ideal actuator disc with a non-rotating wake, there is a change in pressure power as well as kinetic power between far upstream and far downstream. The theory which considers this is usually referred to as 'general momentum theory' and has been the subject of extensive discussion [28, 40–42, 44]. Standard BEM models, such as those developed in Sections 1.8.1–1.8.4, consider wake rotation to the extent of relating the tangential velocity developed at the rotor plane and its associated induction factor to the rotor torque, but they ignore power terms associated with rotational kinetic energy and suction potential energy of the wake. An extensive review comparing BEM models including general momentum theory is available in Sørensen [28].

1.8.6 BEM in Augmented Flow

The generalised actuator disc results of Section 1.7 can be used to derive a generalised BEM that will assist in the optimisation of rotors in ducts or diffusers. In order to revise the BEM equations for generalised flow conditions, consider first the elemental thrust and axial momentum balance:

The mass flow rate through the rotor plane is $\rho(2\pi r dr)$ $\{U(1-a)F\}$. The total change in flow velocity between far upstream and far wake (see Table 1.4) is:

$$dU = U\left\{1 - \left(\frac{1-2a+a_0}{1-a_0}\right)\right\} = \frac{2U(a-a_0)}{(1-a_0)} \tag{1.54}$$

However, considering the thrust force on the rotor alone (see Equation 1.41):

$$dT = 4\pi\rho r U^2 \frac{(a-a_0)(1-a)}{(1-a_0)^2} F\,dr \tag{1.55}$$

Equation 1.42 is unchanged and hence

$$dQ = 4\pi\rho r^3 U a' \omega (1-a) F\,dr \tag{1.56}$$

Equations 1.41, 1.42 and 1.45 are also unchanged. The tangential induction factor a' may be approximated by neglecting drag and generalised as

$$a'(1+a') = \frac{(1-a)(a-a_0)}{(1-a_0)\lambda^2 x^2} = \frac{C_t(1-a_0)}{4\lambda^2 x^2} \tag{1.57}$$

The further development of the generalised BEM model is simplest if a_0 is assumed to be a suitably averaged constant value over the rotor disc and that is tacitly assumed in the following analyses. However, there is no requirement for this and a variation of $a_0 \equiv a_0\ (r, \theta)$ may be defined over the rotor disc. The equation system in the generalised flow case may be solved by iterative numerical methods in the same way as in standard BEM. The associated non-dimensional lift distribution is

$$\Lambda(\lambda, x) = \frac{2\pi C_t}{B\lambda(1+a')\sqrt{(1-a)^2 + \lambda^2 x^2 (1+a')^2}} \frac{F}{\left[1 + \dfrac{(1-a)}{k\lambda x(1+a')}\right]} \tag{1.58}$$

For an optimum rotor, $a = a_m = (1+2a_0)/3$ and $C_t = 8/9$.

If the maximum lift-to-drag ratio of a chosen aerofoil section occurs at an angle of incidence $\alpha = \alpha_{0,}$ then the optimum twist distribution is given as:

$$\psi(x) = \tan^{-1}\left\{\frac{2(1-a_0)}{3\lambda x(1+a')}\right\} - \alpha_0 \tag{1.59}$$

The optimum twist distribution will evidently vary with a_0 and hence may vary significantly according to the nature of the system affecting the rotor plane induction. Suppose there is substantial flow augmentation at the rotor plane. As $C_t = 8/9$ universally, the rotor is optimally loaded at exactly the same value of thrust coefficient and thrust as in open flow with no augmentation system present. This implies that the blade elements must be pitched much further into the flow direction so that a reduction in the lift component producing thrust exactly compensates for the potential increase in thrust due to the augmented local flow velocity. However, in this situation there is then a much larger lift contribution to rotor torque than in open flow. This corresponds to the increased power performance coefficient, which may exceed the Betz limit in proportion to the flow augmentation achieved.

The usual actuator disc theory, whether standard or generalised, considers only inviscid flow. In order to be more realistic and useful for design calculations, empirical modelling is introduced to represent the thrust coefficient in the turbulent wake state. Experimental validation for systems with concentrators is not yet available, and so the results derived represent no more than a consistent extension from the standard open flow model to the generalised actuator disc theory.

If a is the induction at the rotor plane in open flow, then the transformation, $a \to (a - a_0)/(1 - a_0)$ determines the value of axial induction at a plane (not the rotor plane) in constrained flow where the induction is half of that in the far wake. However, as is explained in Jamieson [36], the value of thrust coefficient, C_t, is independent of location in the system. Therefore, this transformation may be employed to determine an expression for thrust coefficient that is applicable at the rotor plane.

In open flow, various formulations are employed to modify the thrust coefficient equation of the inviscid flow actuator disc as the rotor approaches the turbulent wake state. DNV GL's commercial BEM software package, *Bladed*, defines thrust coefficient, C_t, as:

$$C_t = 4a(1 - a) \quad \text{for } 0 \le a \le 0.3539 \tag{1.60}$$

$$C_t = 0.6 + 0.61a + 0.79a^2 \quad \text{for } 0.3539 < a \le 1 \tag{1.61}$$

In generalised flow states, applying again the transformation of Equation 1.90 results in the equations:

$$C_t = \frac{4(a - a_0)(1 - a)}{(1 - a_0)^2} \quad \text{for } 0 \le a \le a_0 + 0.3539(1 - a_0) \tag{1.62}$$

$$C_t = 0.6 + 0.61\left\{\frac{a - a_0}{1 - a_0}\right\} + 0.79\left\{\frac{a - a_0}{1 - a_0}\right\}^2 \text{for } a_0 + 0.3539(1 - a_0) < a \le 1 \tag{1.63}$$

Equation 1.81 does not accurately accord with BEM theory as reflected in Equation 1.85, where the tip effect modifies the thrust coefficient. Thus, the method of application is to factor the C_t in the BEM solutions as a ratio of Equation 1.61 or 1.63 to the corresponding actuator disc Equations 1.60 and 1.62.

In open (unconstrained) flow, the thrust coefficient is essentially unique and optimum at 8/9 at least in the ideal inviscid flow case. However, as is elaborated in Jamieson [36], in constrained flow, the thrust coefficient is a system property. Irrespective of rotor efficiency, C_t in an ideal system is optimally 8/9 and maximises C_p at that value. If the system is not *ideal* in the optimal rotor loading state (which for a diffuser would mean that the diffuser is not fully optimised for the flow field that will develop in operation at a rotor thrust coefficient of 8/9), then the C_t that maximises C_p will be <8/9 and the associated maximum C_p will be less than it would be in an ideal system. On the other hand, any external mass flow (i.e. flow not passing through the rotor) that influences the overall energy exchange, for example, by assisting wake transport, may increase the optimum C_t at the rotor plane to above 8/9. Results of Phillips *et al.* [29] suggest that in a well-designed diffuser, an optimum C_t of around unity may be achieved.

Great care is required in applying generalised BEM to real systems, but the new theory offers a rationalised approach and parametric insight for the optimisation of rotor design in flow concentrators that has not been previously available. The general approach as in Jamieson [39] will be to replace a_0 with $\eta(a)\ a_0$, where $\eta(a)$ is a system efficiency function to be defined from empirical information, CFD analyses or otherwise. Also, the estimation of a_0 is not straightforward, as is discussed in Jamieson [39].

Nevertheless, the introduction of the variable a_0 characterising flow augmentation in conjunction with the indicated generalisation of the thrust coefficient indicates an extension of the BEM theory, which is simple to implement and can address the design of rotors in flow concentrators.

It is also important to be aware of systems where ducted rotors may be used, and the generalised BEM theory developed here will not be applicable as in the case of a tidal turbine where distances from the free water surface and sea bed are not large compared to the rotor dimensions. In such a case, Bernoulli's equation with only pressure and velocity terms (the usual basis of wind turbine actuator disc models) is insufficient and an adequate model [45] must account for buoyancy terms as the pressure drop behind the turbine will induce a local drop in sea surface level.

The analytical relationships developed in the foregoing discussion of BEM theory can be bypassed in the use of the usual numerical methods for BEM solutions. However, identification of explicit formulae is considered to be of great value in design development, facilitating preliminary parametric studies that provide insight into how some of the key variables in rotor design may influence performance. This will be revisited later in the context of specific case studies.

1.8.7 Closed-Form BEM Solutions

With the assumption advocated by Wilson *et al.* [41] that drag should be neglected in evaluating the induction factors, a closed-form solution to the BEM equations can be obtained. This has been previously established [43], but the following presentation provides a form that, with piecewise representation of aerofoil characteristics, could be adapted to represent aerofoils with nonlinear lift characteristics (stall). Neglecting the tip loss, F, the term with lift-to-drag ratio k on the assumption that $k\lambda$ is very large and, initially at least, also neglecting the tangential induction factor which is very small in effective operating states, Equation 1.50 reduces to

$$\Lambda(\lambda, x) = \frac{8\pi a(1-a)}{B\lambda\sqrt{(1-a)^2 + \lambda^2 x^2 (1+\acute{a})^2}}$$

which is equivalent to;

$$\frac{c(\lambda, x)\mathrm{Cl}}{R} = \frac{8\pi a \sin(\phi)}{B\lambda} \tag{1.64}$$

Let us now represent the lift coefficient, $\mathrm{Cl}(\alpha)$, as

$$\mathrm{Cl}(\alpha) = \mathrm{Cl}_0 \sin(\alpha + \alpha_0) \tag{1.65}$$

This representation of lift coefficient provided by Equation 1.65 is effectively linear over the usual range of attached flow and the constant, α_0, can represent the effect of camber in providing positive lift at zero flow incidence. The lift slope Cl_0 may be represented as $2\pi k_0$, where k_0 is a correction factor to the ideal lift slope value of 2π. For example, $k_0 = 1.062$ for a NACA 63421 section that may typically be used on a large HAWT.

Relative to the rotor plane, a total equivalent pitch angle may be defined as;

$$\theta(x) = \theta_t(x) + \theta_s + \theta_p - \alpha_0 \tag{1.66}$$

In its most general form, θ_s is a set angle of the blade relative to the rotor plane at zero degrees pitch and θ_p is the applied pitch angle (relative to the set angle). From Equation 1.65, noting from Figure 1.16 that $\alpha(x) + \alpha_0 = \phi(x) - \theta(x)$ where ϕ is the inflow angle, the axial induction, a, may be expressed as

$$a(x) = \left(\frac{B\mathrm{Cl}_0 \lambda c(x)}{8\pi R}\right) \frac{\sin(\phi(x) - \theta(x))}{\sin(\phi(x))}$$

$$a = \frac{k_1 \lambda \sin(\phi - \theta)}{\sin(\phi)} \quad \text{where } k_1(x) = \frac{B\mathrm{Cl}_0 c(x)}{8\pi R} \tag{1.67}$$

In Equation 1.67, for convenience, the explicit dependence of variables has been removed. Now the flow triangles of Figure 1.16 provide a second equation for the axial induction factor, a.

$$a = 1 - \lambda x \tan(\phi) \tag{1.68}$$

In eliminating a from Equations 1.67 and 1.68, a quadratic equation in $\sin(2\phi)$ is obtained with the solution:

$$\sin(2\phi) = \left\{ \frac{\sqrt{(-c_0^2 + c_1^2 + 1)} - c_0 c_1}{c_1^2 + 1} \right\} \tag{1.69}$$

where $c_0 = \dfrac{(k_1 \sin(\theta) - x)}{(k_1 \sin(\theta) + x)}$ and $c_1 = \dfrac{(1 - k_1 \lambda \cos(\theta))}{(k_1 \sin(\theta) + x)\lambda}$

Hence, the inflow angle, angle of attack, axial induction factor and lift coefficient can be calculated at any radius fraction, x. To complete a BEM analysis, aerofoil drag may be represented as a function of angle of attack, as, for example, in Equation 1.70 (which is a curve fit representative of data for a NACA 63421 aerofoil).

$$\mathrm{Cd}(\alpha) = 0.4147\,\alpha^2 - 9.775 \times 10^{-4}\alpha + 5.388 \times 10^{-3} \tag{1.70}$$

The lift-to-drag ratio can then be computed for any given α and the tangential induction factor, $\acute{a}$, from Equation 1.52. Accepting some further approximation in results, the tip loss factor (such as in the Prandtl form of Equation 1.71 may also be added. In estimating the induction factors, drag is in effect set to zero in Equations 1.44 and 1.45. It must naturally be accounted for in later calculations of rotor torque, power and loads.

This 'closed-form' BEM analysis, at least for operating states not too far off design, gives only slightly different results from iterative solutions that include drag in estimating the induction factors such as DNV GL code Bladed. For use as computer code, it is probably no more efficient than the arguably more exact iterative solutions which can usually converge very rapidly. It is occasionally useful for parametric analysis in enabling analytic rather than numerical investigations.

1.9 Optimum Rotor Design

1.9.1 Optimisation to Maximise C_p

Optimum states are simpler to describe than general conditions. An analogy is that only three coordinates will define the summit of a hill whilst infinitely many may be required to characterise the whole surface. A natural assumption, having chosen a particular wind turbine system scale and rotor diameter, is to consider as optimum an aerodynamic design that will maximise power performance by maximising the rotor power coefficient, C_p.

In the optimum state, for typical rotors designed for electricity production with design tip speed ratios above 6, the tangential induction factor, a', should be small over the significant parts of span ($x > 0.2$). It may be neglected with little loss of accuracy in $\Lambda(\lambda, x)$ or calculated from Equations 1.51, 1.52, or 1.53.

The actuator disc result of Betz [46] establishes an optimum rotor thrust loading corresponding to a value of the thrust coefficient, $C_t = 8/9$. This implies an optimum lift force on each blade element, which in effect specifies the product, cC_L, in Equation 1.41. Referring to Equation 1.42, it is plausible that with cC_L fixed, performance is maximised if C_D is minimum and hence k is maximum. Thus, in the optimum operational state of a wind turbine rotor, each blade element operates at maximum lift-to-drag ratio and the only aerofoil data required to define this state therefore is the maximum lift-to-drag ratio, k, and the lift coefficient, C_L, associated with this maximum lift-to-drag ratio for each element over the span of a blade. Optimum performance at maximum lift-to-drag ratio is not exactly true (see later discussion around Equation 1.84), but is a satisfactory approximation for mainstream designs with design tip speed ratio above 6.

For a lift-to-drag ratio, $k = 100$, design tip speed ratio, $\lambda = 9$ and considering an optimum rotor with $a = 0.3333$ at mid span where $x = 0.5$, Equations 1.51 and 1.53 give values for a' of 0.01010 and 0.01097 a difference in the optimum rotor state of around 10% albeit in a rather small quantity compared to the axial induction, a.

The square bracketed term in the denominator of Equation 1.50 which contains the lift-to-drag ratio k is effectively unity over the significant region of span for typical modern large rotors with design tip speed ratio >6 and $k \geq 100$.

The lift produced by an aerofoil section can be associated with a bound circulation which is virtual over the span of the blade but becomes a real vortex at the end of the blade where there is no material to support a pressure difference. The strength of this vortex depends on blade number and blade solidity, and it is through models of this 'tip effect' that the effect of the blade number on rotor performance is expressed in BEM theory. Various tip effect models have been developed (see Section 1.10.3), the most rigorous by Goldstein [47]. The most commonly used model in BEM theory is from Prandtl (see Wilson [41] for example) and that model is adopted in the following analyses.

Adopting the Prandtl tip factor, $F = (2/\pi)\cos^{-1}(e^{-\pi s/d})$ where $d = 2\pi R(1 - a)/(B\lambda)$ and $s = (1 - x)R$:

$$F = \frac{2}{\pi}\cos^{-1}\left[\exp\left\{-\frac{(1-x)B\lambda}{2(1-a)}\right\}\right] \tag{1.71}$$

With the assumptions that $a = 1/3$ in optimum operation, that a is constant over the span and knowing the value of lift coefficient at maximum lift-to-drag ratio for the aerofoil section selected at each radial station, Equation 1.50 then defines the chord distribution of an optimum rotor as a function of radius fraction, x and design tip speed ratio, λ. If the approximations of neglecting a', neglecting the very minor effect of drag and neglecting tip effect are combined with the further approximation of neglecting $(1 - a)^2$ in comparison to $\lambda^2 x^2$, Equation 1.50 then reduces to

$$\Lambda(\lambda, x) = \frac{8\pi a(1-a)}{B\lambda^2 x} = \frac{16\pi}{9B\lambda^2 x} \tag{1.72}$$

Equations similar to Equation 1.72 have appeared in various forms, in Gasch and Twele [48], Burton and Sharpe [49], and are easily understood intuitively. Lift per blade element is proportional to dynamic pressure and chord width. Dynamic pressure on a blade element is proportional to the square of the inflow velocity, which is predominantly the in-plane velocity when $\lambda > 6$. Thus, to maintain total rotor lift at the appropriate fixed optimum value, Λ (λ, x) must approximately vary inversely as $B\lambda^2 x$.

Equation 1.50 (or its simplified forms such as Equation 1.72) allows the optimum chord distribution of a blade to be developed given a selection of aerofoil types that will then define at each radial station, x, the maximum lift-to-drag ratio, k, the associated design lift coefficient, C_L and the corresponding angle of incidence, α_0. An optimum blade twist distribution is then determined referring to Equation 1.43 and setting $a = 1/3$ as:

$$\theta(x) = tan^{-1}\left\{\frac{2}{3\lambda x(1+a')}\right\} - \alpha_0(x) \cong \frac{2}{3\lambda x} - \alpha_0(x) \tag{1.73}$$

As far as optimal blade shape is concerned, the simplified Equation 1.72 predicts the chord distribution very well over the extent of span that most matters. It would be usual in real designs to round the tip in a way that may be guided by practical experience or CFD analyses and, for practical reasons associated with manufacture and/or transportation, to limit the chord to much less than ideal values inboard of say 20–25% span. With the chord being so limited, and the sections normally transitioning to a cylindrical blade root end, there is then no point to continue the twist distribution near the blade root to the very high angles that would be predicted by Equation 1.73. In that case, the approximate form of Equation 1.73 is a good estimate over the aerodynamically active part of the rotor.

As was discussed, the optimum lift force on each blade element specifies the product, cC_L, in Equation 1.42. This means that the chord width can be optimised structurally if aerofoils are available or can be designed with suitable values of design lift coefficient C_L. Thus, as is discussed further in Chapter 2, for the same blade design tip speed ratio, aerofoils with high or low design C_L can enable slender or wide optimum blades.

There is however constraint on having rapid changes in the spanwise variation of C_L. A basic principle is that it is generally undesirable to have rapid changes in section lift (specifically lift and not lift coefficient) along the span of the blade. The trailing vortices which generate induced drag (or the induction factor for a rotor) are proportional to the spanwise gradient of lift (actually circulation but effectively the same). A sudden change in blade chord is undesirable structurally and aerodynamically; this implies that C_L should not change abruptly since the relative inflow velocity varies only gradually with radial position. It is therefore usually assumed[9] that a constant C_L is desirable over most of span with a smooth reduction to zero at the tip.

Having characterised the optimum lift distribution as in Equation 1.50, expressions generally useful for parametric studies are now derived for the power coefficient, thrust coefficient and out-of-plane bending moment coefficient (to be defined). The torque coefficient, $C_q = \frac{Q}{0.5\rho U^2 \pi R^3}$, where Q is the rotor torque, is sometimes useful in evaluating the self-starting capability of wind turbines and is trivially related to the power coefficient as $C_q = \frac{C_p}{\lambda}$.

1.9.2 The Power Coefficient, C_p

Returning to Equation 1.42:

$$dQ = \frac{1}{2}\rho W^2 Bcr(C_L \sin\varphi - C_D \cos\varphi)dr \tag{1.74}$$

Hence elemental power is

$$dP = \frac{1}{2}\rho W^2 Bcr(C_L \sin\varphi - C_D \cos\varphi)\omega dr \tag{1.75}$$

$$= \frac{1}{2}\rho\left(\frac{W}{U}\right)^2 R^2 V^3 \Lambda(\lambda, x)B\left(\sin\phi - \frac{\cos\phi}{k}\right)\lambda x dx \tag{1.76}$$

and the rotor power coefficient is

$$C_p = \frac{B}{\pi}\int_0^1 \Lambda(\lambda, x)\left(\frac{W}{U}\right)^2\left(\sin\phi - \frac{\cos\phi}{k}\right)\lambda x dx \tag{1.77}$$

Substituting for W/U, sin φ and cos φ from Figure 1.16 and for $\Lambda(\lambda, x)$ from Equation 1.50:

$$C_P = \frac{B}{\pi}\int_0^1 \frac{8\pi a(1-a)F}{B\lambda(1+a')}\frac{\lambda\left\{(1-a) - \frac{\lambda x(1+a')}{k}\right\}xdx}{\left\{1 + \frac{(1-a)}{k\lambda x(1+a')}\right\}}. \tag{1.78}$$

Considering a rotor without tip effect, assuming a constant over the rotor span, neglecting a' and neglecting also $\frac{(1-a)}{k\lambda x(1+a')}$:

$$C_p = 8a(1-a)\int_0^1 \left\{(1-a) - \frac{\lambda x}{k}\right\}xdx \tag{1.79}$$

9 The optimum spanwise distribution of circulation or lift on a fixed wing is a smooth elliptic variation (which was provided uniquely at all angles of attack by the Spitfire wing), but there may not be any simple theory to define the optimum shape for a rotor.

and hence:

$$C_p = 4a(1-a)^2\left[1 - \frac{2\lambda}{3k(1-a)}\right] \tag{1.80}$$

Equation 1.80, as it must, tends to the actuator disc result of Betz as $k \to \infty$. With k finite, it is similar to a limiting case derived by De Vries [50] which arose from a quite different beginning in the context of BEM theory for vertical axis wind turbines. De Vries' equation is

$$C_p = 4a(1-a)^2 - \frac{BcC_D\lambda^3}{2R} \tag{1.81}$$

Noting that $\frac{BcC_D\lambda^3}{2R} = B\left(\frac{cC_L}{R}\right)\frac{\lambda^3}{2k}$ and also considering Equation 1.72, the Equations 1.80 and 1.81 have a similar form.

Returning to Equation 1.78, the general expression for C_p can be expressed as:

$$C_p(\lambda) = \int_0^1 \frac{8a(1-a)F[k(1-a) - \lambda x(1+a')]\lambda x^2}{[k\lambda x(1+a') + (1-a))]}dx \tag{1.82}$$

Equation 1.82 is a rigorous BEM relationship defining C_p first published, Jamieson [51], without derivation. As was mentioned in connection with Equation 1.51, the lift-to-drag ratio, k, is a function of angle of attack $\alpha(\mathrm{x}) = \varphi(\mathrm{x}) - \theta(x) - \psi$ and the flow angle $\varphi\ (x)$ is therefore implicitly present in Equation 1.82.

However, in the optimum rotor state, for typical design tip speed ratios above, say, about 6 and with typical aerofoil selections for large HAWTs, it is a very good approximation to assume that all the blade elements operate at their maximum lift-to-drag ratio, $k \equiv k(x)$ and, using Equation 1.51 or 1.52 to determine a', Equation 1.82 can then be directly integrated. Hence, maximum C_p may be expressed as a function of tip speed ratio and lift-to-drag ratio as in Figure 1.17. Although for convenience in the calculations presented in Figure 1.17, the lift-to-drag ratio is treated as constant over the blade span, there is no requirement for this to be the case. If k is defined as a function of x, Equation 1.82 can be used for a rotor with differing aerofoil characteristics over the span, as is usually the case on account of thickness-to-chord ratio decreasing from root to tip.

A chart such as Figure 1.17 has been published previously [52], but the results were determined by numerical solution of the BEM equations and not from an explicit formula. After such an exercise, Wilson *et al.* [41] fitted data with the formula (Equation 1.83) which was claimed valid for $4 \le \lambda \le 25$, and $k = C_l/C_d \ge 25$ but restricted to three blades maximum.

$$C_{p\,\max} = \left(\frac{16}{27}\right)\lambda\left[\lambda + \frac{1.32 + \left(\frac{\lambda - 8}{20}\right)^2}{B^{2/3}}\right]^{-1} - \frac{(0.57)\lambda^2}{\frac{C_l}{C_d}\left(\lambda + \frac{1}{2B}\right)} \tag{1.83}$$

Some general similarity between this empirical relation Equations 1.81 and 1.78 may be noted with the additional complexity in Equation 1.81 taking account of tip effects over the range of applicability.

It will be evident (Figure 1.17) that for any given blade number, B, and maximum lift-to-drag ratio, k, there is a unique optimum value of tip speed ratio, λ to maximise C_p. Figure 1.18 shows C_p max as a function of design tip speed ratio for a range of lift-to-drag

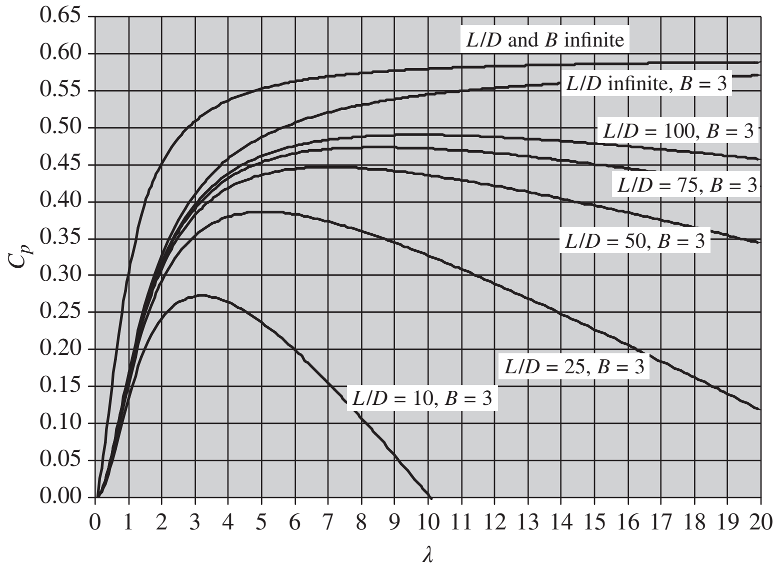

Figure 1.17 C_p max versus tip speed ratio for various lift-to-drag ratios.

ratios and blade numbers. As is confirmed in Figure 1.18 (and also in Figure 1.17), a typical state-of-the-art blade for a large wind turbine designed for a tip speed ratio of around 9 and with average equivalent maximum lift-to-drag ratio around 100 will achieve C_p max of ~0.5. While Figure 1.17 shows appropriate trends, without a full solution of the BEM equations, Equation 1.82 using the assumption of k constant at a maximum value for the chosen aerofoils will only predict C_p curves accurately in the region of C_p max.

Figure 1.18 clarifies an important point that to maximise the benefit from aerofoils that may achieve higher lift-to-drag ratios, it is important to design new (higher) optimum tip speed ratios. Figure 1.18 also provides a clear and immediate indication of how optimum one-, two-, three- or multi-bladed rotors will compare in power performance for any given choice of aerofoils, whilst Figure 1.17 clarifies the penalties that may apply in operating at non-optimum combinations of lift-to-drag ratio and design tip speed ratio.

Equation 1.82 shows that C_p is a complex function of the axial induction, a. The result that $a = 1/3$ results in maximum rotor C_p was based on simple actuator disc theory (Equation 1.11) and this clearly cannot be exactly true for Equation 1.82. It may also be noted that from Equation 1.74, it is only plausible and not rigorous that maximising $k = C_l/C_d$ will maximise the torque on each blade element as the elemental torque clearly also depends on flow angle, φ and how it may vary with k in the course of a full solution of the BEM equations. Considering Equation 1.76, a power coefficient can be defined local to each blade element as:

$$C_p(r, a, k) = \frac{dP(r, a, k)}{0.5\rho U^3(2\pi r\, dr)} \tag{1.84}$$

A strict optimisation according to the BEM theory presented will maximise $C_p\,(r, a, k)$ separately on each blade element. This results in a varying spanwise and k near to maximum but not absolutely maximum on each aerofoil section. For typical large

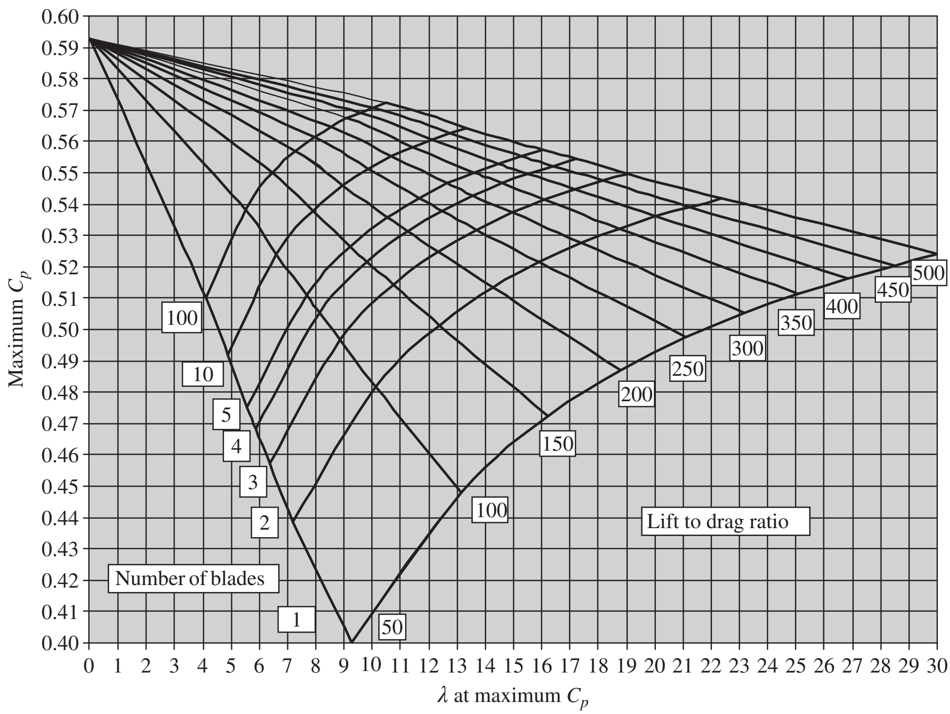

Figure 1.18 Influence of blade number and lift-to-drag ratio on maximum C_p.

electricity producing wind turbines with design $\lambda \geq 6$ and $k \geq 100$, in an ideal optimum blade design, a is a little different from 1/3 over most of the span and k is very close to the maximum for each aerofoil section. These effects are rather more significant, however, for a rotor based on aerofoils with low lift-to-drag ratio, for example, sailcloth blades or plate blades. The non-uniformity of an optimum distribution of axial induction is not of practical importance for optimum rotor design because of the limitations of BEM theory in its present form. Other issues appear in more accurate optimisation methods (see Section 1.10.4). However, based on the BEM equation system in a standard form, the non-uniformity of axial induction (i.e. not exactly constant at a value of 1/3 over the whole span) of an optimum rotor is a consistent outcome and is mentioned for that reason.

1.9.3 Thrust Coefficient

In a similar way to the derivation of maximum C_p from Equations 1.74–1.82, the associated thrust coefficient can be determined as

$$C_T = \int_0^1 8a(1-a)Fxdx \tag{1.85}$$

In the limit of no tip loss ($F = 1$), the familiar actuator disc formula, $C_T = 4a(1 - a)$, is recovered with $C_T = 8/9$ for an optimum rotor. Equation 1.85 has a much simpler form than Equation 1.82. The thrust coefficient is a *system* property dependent on rotor loading but independent of the efficiency of the rotor in power conversion. It is therefore unaffected by lift-to-drag ratio or the tangential induction factor and dependent only on the state of rotor loading characterised by the axial induction over the rotor plane which is naturally influenced by the tip effect.

1.9.4 Out-of-Plane Bending Moment Coefficient

The steady-state out-of-plane bending moment of an optimised blade in operation at its design tip speed ratio below rated wind speed and the introduction of pitch action may be derived from any standard BEM code and has a characteristic shape as in Figure 1.19. For typical large-scale electricity generating wind turbines, which are well optimised rotor designs with design tip speed ratios above 6, the shape is largely independent of design specifics and can usually be very well approximated by a cubic curve. Such representations have been convenient in studies developing blade designs embodying passive aeroelastic control (e.g. with flap-twist coupling as in Maheri [53]), where a simplified representation of blade loading is useful. BEM theory provides a simple derivation of the result as follows.

Defining a dimensionless bending moment coefficient at arbitrary radial distance, r, as $C_M(r) = \frac{M(r)}{(0.5\rho U^2 \pi R^3)}$ and following similar methods of analysis as for C_p in Equations 1.74–1.82 lead to:

$$C_M(r) = \frac{8a(1-a)}{B} \int_x^1 \frac{F(y)}{\left\{(1+a')\lambda y + \dfrac{(1-a)}{k}\right\}} \left\{\lambda y + \frac{(1-a)}{k}\right\} (y-x) y dy \tag{1.86}$$

Neglecting a' in comparison to unity gives

$$C_M(x) = \frac{8a(1-a)}{B} \int_x^1 F(y)(y-x) y dy \tag{1.87}$$

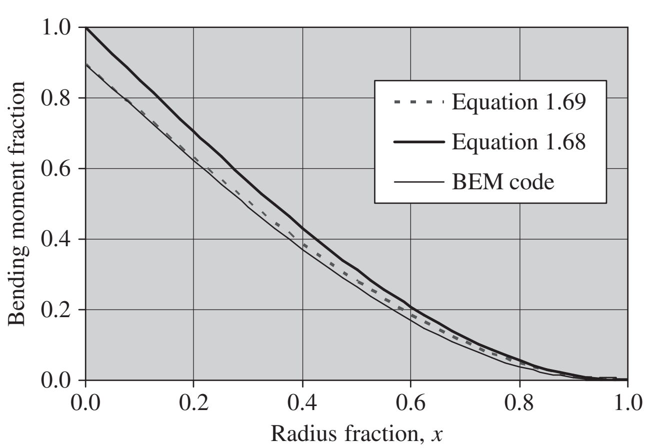

Figure 1.19 Out-of-plane bending moment shape functions.

Considering the case with no tip effect, where $F(y) = 1$:

$$C_M(x) = 4a(1-a)\left\{\frac{1}{3B}(2 - 3x + x^3)\right\} \tag{1.88}$$

And for an optimum rotor, taking $a = 1/3$:

$$C_M(x) = \frac{16}{27B}\left\{\frac{(x-1)^2(x+2)}{2}\right\} \tag{1.89}$$

For a typical conventional three-bladed wind turbine, Equation 1.89 has the appropriate cubic shape but, because the bending moment is most heavily weighted by the loading which is farthest outboard, the tip effect is very significant in relief of blade root bending moment.

Wilson (see Spera [52], Chapter 5, p. 261) and Milborrow [54] (a paper offering a variety of useful simplified parametric equations for blade loads) have previously derived an equation similar to Equation 1.89. Wilson noted that this relationship predicted values significantly greater than measured blade bending moment data [55] from the Mod-2 HAWT. He further observed that the Mod-2 blade design was far from an optimised configuration and described Equation 1.89 as 'an upper bound' which it is for an optimum rotor without tip loss. However, noting the more general form of Equation 1.88, the bending moment coefficient is unsurprisingly related to the thrust coefficient which is not maximised at $a = 1/3$ even in the ideal inviscid model without considering higher loadings that may result in the turbulent wake state. Thus, suboptimal rotors may have bending moment characteristics that exceed (or are within) the predictions of Equation 1.89.

A direct application of Equation 1.89 will overestimate the moment at shaft centreline of an optimum three-bladed rotor with a design tip speed ratio of $\lambda = 7$ by about 13%. Equation 1.87 is therefore not immediately appropriate for use in parametric studies without some adjustment to account for the tip effect.

Equation 1.90 is a useful approximation to Equation 1.83, which can represent the blade root moment quite accurately when (as is the case for mainstream electricity generating wind turbines) the product of blade number and design tip speed ratio, $B\lambda > 10$.

$$C_M(x) = \frac{16}{27B}G(B\lambda)f(x) \tag{1.90}$$

where

$$G(B\lambda) = 5.5744 \times 10^{-7}B^3\lambda^3 - 8.2871 \times 10^{-5}B^2\lambda^2 + 4.4085 \times 10^{-3}B\lambda + 2.3245 \times 10^{-1} \tag{1.91}$$

and

$$f(x) = \frac{(x-1)^2(x+2)}{2} \tag{1.92}$$

In retaining the simple cubic function, $f(x)$, and providing an accurate match to the blade root bending moment, Equation 1.90 is somewhat conservative in blade out-of-plane bending moment estimates on the outboard blade. Accuracy in estimation of blade root bending moment is probably of greatest interest in parametric studies and, for a three-bladed wind turbine with $\lambda = 7$, Equation 1.90 gives C_M (0) as 0.8809, whilst integration of Equation 1.86 using the Prandtl tip loss factor gives a corresponding value of 0.8827.

1.9.5 Optimisation to a Loading Constraint

As is discussed in Chapter 9, the most prevalent system optimisation criterion is to minimise cost of energy (COE). Maximising rotor aerodynamic performance is certainly a natural design objective but may not be overall optimum in minimising COE. Snel [56] noted that at peak C_p (corresponding in the ideal case to an axial induction factor, $a = 1/3$) the thrust coefficient, C_t is rising rapidly so that it may be beneficial to back off maximum C_p a little, sacrificing a little power in order to reduce loads rather more substantially. This idea has been implemented in many past rotor designs but not to the extent of having aerodynamic designs targeting a very much lower induction, a concept more recently explored by Chaviaropoulos and Voutsinas [57]; and this idea was taken further including specialised aerofoil design for such a rotor in the Innwind.EU project [58]. The possibility of a COE benefit in a design for low axial induction and reduced C_p max was investigated. The aim is to have a larger and more productive rotor able to operate at similar load levels to one designed for C_p max at $a = 1/3$.

The essence of this can be derived very simply considering the ideal actuator disc equations for C_p and C_t. From Equation 1.88, the steady-state out-of-plane bending moment, M, at fixed wind speed U is seen to be proportional to the cube of radius, R, and to the thrust coefficient, C_t. Thus,

$$M \propto C_t R^3 \propto a(1-a)R^3$$

Suppose an optimum rotor design is developed to maximise power on the basis that a and R may vary while M is kept constant. Thus,

$$M \propto C_t R^3 \propto a(1-a)R^3 = k_m \text{ (constant)} \tag{1.93}$$

Equation 1.93 holds true for the out-of-plane bending moment at any blade radius when a is the associated local induction but, for the present analysis, consider M to be evaluated at the blade root. The power at the same wind speed, P, is given as

$$P \propto C_p R^2 \propto a(1-a)^2 R^2 \tag{1.94}$$

And thrust, T, is given as

$$T \propto C_t R^2 \propto a(1-a)R^2 \tag{1.95}$$

The variation of power and thrust with a and R may be considered. As a and R are now related through M being constant, $P(a)$, $R(a)$ and $T(a)$ may be determined. From Equations 1.93 and 1.94; $P = k\, a^{1/3}(1-a)^{4/3}$ (with k, another constant) and

$$\frac{dP}{da} = \frac{k}{3} a^{-2/3}(1-a)^{1/3}(1-5a) \tag{1.96}$$

Hence, for P to be maximum,

$$a = \frac{1}{5}$$

Applying the subscript s to values associated with a standard rotor design ($a = a_s = 1/3$), when P is maximum:

$$\frac{R}{R_s} = \left\{ \frac{a_s(1-a_s)}{a(1-a)} \right\}^{1/3} = 1.116$$

$$\frac{P}{P_s} = \frac{a(1-a)^2}{a_s(1-a_s)^2}\left(\frac{R}{R_s}\right)^2 = 1.076$$

$$\frac{T}{T_s} = \frac{a(1-a)}{a_s(1-a_s)}\left(\frac{R}{R_s}\right)^2 = 0.896$$

General trends of R, P, M and T relative to unit values of the standard rotor are presented in Figure 1.20.

The analysis indicates that a rotor designed for an axial induction factor of 0.2 that may be 11.6% larger in rotor diameter can operate with 7.6% increased power and 10% less thrust at the same level of blade rotor out-of-plane bending moment as the baseline design. The rotor diameter is larger by 11.6%, but this does not produce additional power proportional to the 25 % swept area increase because a lower optimum induction of $a = 0.2$ is intrinsic in the trade-off and the limiting rotor power coefficient is reduced from the Betz limit of 0.593 to a value $C_p = 4a(1 - a)^2 = 0.512$.

A somewhat more detailed and realistic analysis will modify these numbers, but Figure 1.20 captures the essence of the low-induction rotor design concept. Designing for the same blade steady-state out-of-plane bending load level, say, at rated power is not necessarily the overall optimum solution for minimum system COE but it is a clear basis to investigate more deeply whether designs that target a significantly lower induction than 1/3 may reduce COE. There is reduced rotor thrust associated with maximum power (compared to a purely aerodynamic optimisation with $a = 1/3$) and, in consequence, wind farm wake losses may be reduced. A key issue for the low-induction design concept is whether the larger rotor can always defend against critical load increases over the full spectrum of operating conditions and hence avoid related cost increases.

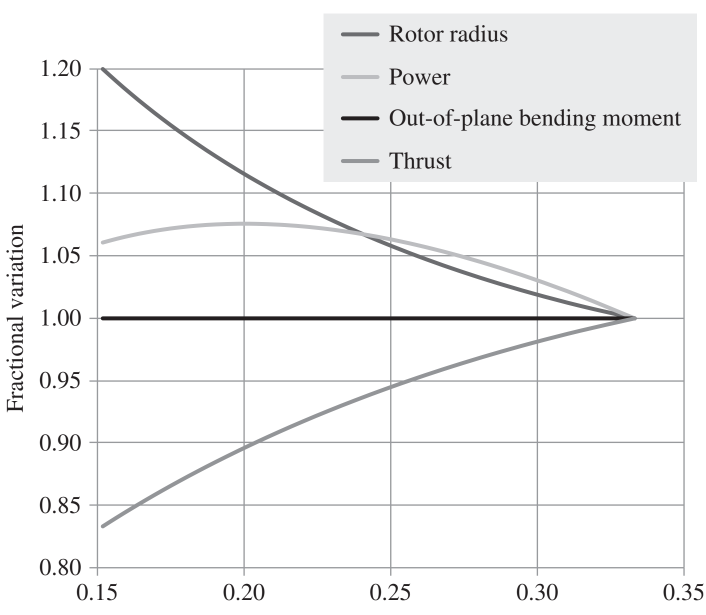

Figure 1.20 Design parameters related to axial induction.

1.9.6 Optimisation of Rotor Design and Hub Flow

Refinements to BEM have been considered [59, 60] in the light of analyses suggesting reduced inboard axial induction associated with reduced pressure near the wake core. These may include viscous effects supported by CFD analysis and are targeted at improving design methods to determine aerodynamically optimum platforms. The following very simplified analysis suggests, however, that such refinements may be pointless unless combined with a model of the flow around some specific hub shape. Flow augmentation benefit from effective design in the hub area may exceed any effects due to wake core suction, while losses in standard design arrangements may conflict with wake suction benefits.

Consider as a reference level an ideal rotor capable of achieving a local C_p on every blade element of 16/27 and hence a complete rotor C_p of 16/27. Now the central region of real rotors varies considerably. There is invariably at least a small nose cone over the hub region. Often, there is an exposed section of blade near the root which is cylindrical having negative aerodynamic performance and creating some drag but no lift. Often, the blade has no positive aerodynamic contribution until beyond 15% span and aerodynamic function is generally reduced inboard of maximum chord which is typically around 25% span.

Let us suppose then that there is a central region of the ideal rotor up to a radius r_a which contributes no aerodynamic power. Then the limiting C_p for the whole rotor is

$$C_p(r_a) = \frac{16}{27}\left(\frac{R^2 - r_a^2}{R^2}\right) \tag{1.97}$$

Consider instead having a large aerodynamically shaped nose cone of radius r_h covering all aerodynamically inactive hub and blade parts and which deflects the central flow constructively over the remainder of the aerodynamically active blade. The whole rotor C_p may now be represented as

$$C_p(r_h, k) = \frac{2}{R^2}\int_{r_h}^{R} \frac{16}{27}\left(1 + k\frac{{r_h}^3}{2r^3}\right) rdr \tag{1.98}$$

The explanation for Equation 1.98 defining $C_p(r_h, k)$ is as follows. If potential flow over a 2D object, say a cylinder, is considered, the flow concentration at right angles to the flow direction varies inversely as square of distance r. For a 3D object, say a sphere, the flow concentration varies as inverse cube of distance. The formula bracketed in Equation 1.98 is the standard potential flow solution for a sphere when the coefficient, k, is unity. Thus, a smooth displacement of the central flow outwards with the added mass flow varying as inversely as cube of the radial distance is represented with a coefficient, k, modelling the specific shape of cone as distinct from a spherical cone. According to Section 1.7 and generally accepted wisdom about flow concentration, local C_p will increase directly in proportion to the mass flow increase as is modelled in Equation 1.98.

Losing performance from an area within 20% span incurs ~4% reduction in rotor C_p, whilst deflecting the central flow over working parts of the blades is predicted to give a 1.7% gain for a hub cone of 20% span (assuming k arbitrarily as 0.5). Such a large hub cone seems quite extreme, but note that GE Wind has recently conducted experiments with very large hub cones (Figure 1.21) and with claims for a performance gain

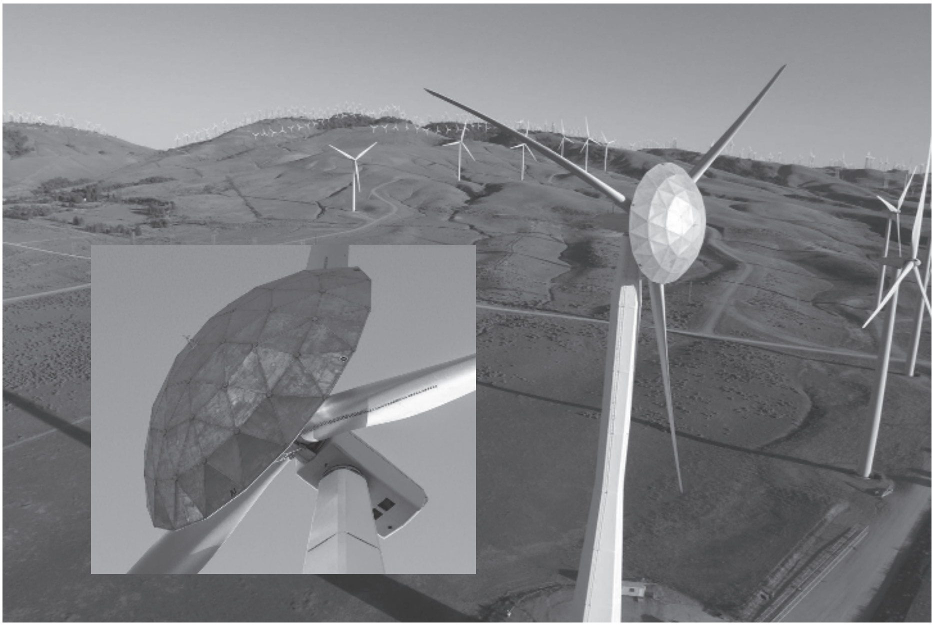

Figure 1.21 GE Wind experimental hub flow system on a 1.7 MW wind turbine. Reproduced with permission of General Electric.

of ~3% [61]. They describe this system as ECO ROTR (Energy Capture Optimization by Revolutionary Onboard Turbine Reshape). The idea that the central flow may be more productively displaced radially outward also appears in studies of downwind turbines by ETH Zurich [62], supported by the Japanese downwind turbine manufacturer, Hitachi. Nacelle blockage preventing flow through the central region of the rotor is found to give small increases in performance.

1.10 Limitations of Actuator Disc and BEM Theory

1.10.1 Actuator Disc Limitations

In spite of the great practical value of his actuator disc concept, Froude was aware of unresolved issues especially in regard to what happens at the edge of the disc. In classical inviscid models, a singularity exists at the edge of the disc because a constant pressure difference across the disc is assumed to exist all the way from the centre to the edge. However, at the edge point, as viewed from outside the disc, the static pressure must in reality have a single unique value. Van Kuik and Lignarolo [23] shows that the isobars converge on the disc edge so that, in the inviscid mathematical model at least, the pressure is infinitely multiple-valued. As far as numerical modelling is concerned, this presents no fundamental problem in getting accurate results near the edge of the disc if the numerical resolution is high enough. It is a quite separate issue how best to model flow at the edge of a real rotor with discrete, finite blade number.

1.10.2 Inviscid Modelling and Real Flows

The actuator disc concept is not in itself limited to inviscid modelling and has been employed in many CFD studies [63], but BEM theory is basically inviscid except that some boundary layer effects are implicit in using aerofoil data accounting for drag and empirical add-ons may be incorporated to approximate modelling of unsteady effects like stall hysteresis. It is rather interesting that a full wake expansion is never observed in real flows due to entrainment and mixing of the external flow through viscous effects. Yet, the inviscid model as represented by standard BEM appears to predict power performance, for example, very well at least for aligned flow conditions in operating states avoiding stall. This BEM model is underpinned by the Betz actuator disc analysis; and after accounting for tip losses and finite aerofoil drag based on 2D wind tunnel data, the Betz limit remains as a very credible upper bound for performance of an open flow rotor.

1.10.3 Wake Rotation and Tip Effect

The so-called tip effect essentially differentiates rotors of similar solidity, aerofoil selection and design speed in terms of blade number. In the limit of an infinite number of infinitely slender blades travelling at infinite rotation speed, all the power is produced without a torque reaction or wake rotation.

Assuming a uniform wind field upstream of the rotor with no intrinsic rotating structures or initial angular momentum, the creation of angular momentum in the wake of the rotor is predicted for all real rotors with a finite number of blades and finite speed, which in turn implies a non-zero torque reaction.

This is not in question, but De Vries [50] and later Sharpe [27] have made the case for the view that wake angular momentum is associated with a reduction in wake core static pressure that arises conservatively from the blade circulation. In reviewing general momentum theory, it is apparent that the wake vortex is conservative as must be any vortex in steady state and in inviscid flow. However, this does not mean that it has no influence on available rotor power. The purely axial flow incident on the rotor provides available power to the rotor through the rotor plane pressure difference and also rotational kinetic power to the wake sharing the rotor plane pressure difference pressure difference and associated power in the ratio $(1 : \acute{a})$ between rotor and wake. Conventional BEM modelling as, for example, presented in Section 1.8 does not consider the effect of wake rotational kinetic power or wake suction power in the overall power balance. In CFD modelling, Madsen *et al*. [59, 60] has supported the De Vries interpretation. This is significant for the physical interpretations underlying BEM theory and for the accuracy of detailed design calculations on rotor aerodynamics. It little affects the top-level parametric analyses and formulae developed in Section 1.9 as applied to rotors with design tip speed ratios above about 6. It will matter especially in detailed aerodynamic design of rotors around the hub and tip areas especially and have substantial implications for rotors with very low design tip speed ratio.

There are a number of tip effect models (e.g. see Shen *et al*. [64]). The Prandtl model has been employed as the simplest available, purely for convenience, having in mind that differentiating these models or getting into accurate correspondence with real tip flows moves into territory where the simple BEM theory is generally inadequate. It should also be noted that there are also a number of different approaches in the application of the tip factors that differ in detail from Equations 1.39 and 1.40 including an elegant model from Anderson [65] which accounts for cyclic variation in the induction factors.

1.10.4 Optimum Rotor Theory

Optimum rotors produced by BEM theory differ a little from those developed with the ideal actuator disc assumption that the axial induction is 1/3 everywhere over the rotor span. These differences are considered unimportant because BEM theory is not accurate enough for them to be really meaningful. Work of Johansen *et al*. [66] on optimum rotor design following from the previous work [59, 60] also suggests that classical BEM solutions for optimum rotors will not be very accurately optimal. This is important both at a fundamental level and for practical detailed design of optimum rotors, but does not particularly undermine the value of equations such as Equation 1.72 for guiding parametric design investigations. As mentioned, using the ideal actuator disc model to optimise a rotor of fixed diameter in order to maximise power leads to the simple result that the axial induction should be 1/3. It is interesting to see that the corresponding optimisation at fixed blade bending moment without constraint on rotor diameter also leads to a simple, elegant but different result that the axial induction should be 1/5.

1.10.5 Skewed Flow

A major weakness of BEM theory is in modelling wind turbines in yawed flow. When the flow is oblique to the rotor plane, there are cyclic variations in angle of attack which can be important especially when flow angles approach stall. The strip theory assumption that the rotor can be analysed as annular elements that are independent of each other is less justifiable. Dynamic stall behaviour and stall hysteresis can have greater effect on rotor performance. Also, in yawed flow there are additional issues about the wake. Does it remain symmetric about the rotor axis or is it skewed in the wind direction? Experimental evidence and CFD analyses indicate the latter and skewed wake correction as, for example, based on Glauert [67] have been applied in using BEM to model yawed flow. BEM theory can adopt simplifying assumptions (such as taking account of the angle of the wind vector in the inflow calculations), can incorporate dynamic stall models and yield useful results. However, in yawed flow, there is much less certainty in basic calculations (even such as the determination of average rotor power) than in cases where the wind direction is normal to the rotor plane. In general, more sophisticated aerodynamic modelling using vortex wake models [9, 68], or CFD is desirable.

1.10.6 Summary of BEM Limitations

The limitations of BEM have been highlighted. CFD- and vortex-theory-based analyses may be more accurate in many circumstances. Nevertheless, although huge advances have been made in recent years and progress will continue, current CFD techniques do not yet solve the Navier–Stokes equations with the same objectivity as Mother Nature. Turbulence, transition and boundary layer modelling remain problematic. Some vortex wake models assume Froude's theorem and some CFD analyses are calibrated to reproduce actuator disc results. It is through a mixture of techniques and convergence of insights coupled with experimental feedback that progress is made.

References

1 Breton, S.-P. (2008) Study of the stall delay phenomenon and of wind turbine blade dynamics using numerical approaches and NREL's wind tunnel tests. Doctoral theses at NTNU, p. 171. ISBN: 978-82-471-1019-5.

2 Chaviaropoulos, P.K. and Hansen, M.O.L. (2000) Investigating three-dimensional and rotational effects on wind turbine blades by means of a quasi-3D Navier Stokes solver. *Journal of Fluids Engineering*, **122**, 330–336.

3 Raj, N.V. (2000) An improved semi-empirical model for 3-D post stall effects in horizontal axis wind turbines. Master of Science thesis in Aeronautical and Astronautical Engineering. University of Illinois at Urhana-Champaign, Urhana, IL.

4 Himmelskamp, H. (1947) Profile Investigations on a Rotating Airscrew. MAP Volkenrode Report and Translation No. 832.

5 Snel, H., Houwink, R., van Bussel, G.J.W. and Bruining, A. (1993) *Sectional Prediction of 3D Effects for Stalled Flow on Rotating Blades and Comparison with Measurements*. 1993 European Community Wind Energy Conference Proceedings, Lubeck-Travemunde, Germany, pp. 395–399.

6 Rasmussen, F., Hansen, M.H., Thomsen, K. *et al.* (2003) Present status of aeroelasticity of wind turbines. *Wind Energy*, **6**, 213–228. doi: 10.1002/we.98

7 Snel, H. (2003) Review of aerodynamics for wind turbines. *Wind Energy*, **6**, 203–211. doi: 10.1002/we.97

8 Ostowari, C. and Naik, D. (1985) Post stall studies of untwisted varying aspect ratio blades with NACA 4415 airfoil section part 1. *Wind Engineering*, **9** (3), 149–164.

9 Simoes, F.J. and Graham, J.M.R. (1990) *A Free Vortex Model of the Wake of a Horizontal Axis Wind Turbine*. Proceedings of the 7th BWEA Conference, Norwich, UK, pp. 161–165.

10 Schreck, S. and Robinson, M. (2002) Rotational augmentation of horizontal axis wind turbine blade aerodynamic response. *Wind Energy*, **5**, 133–150. doi: 10.1002/we.68

11 Hoerner, S.F. (1965) *Fluid Dynamic Drag*, Published by the Author.

12 Krauss, T.A. (inventor) (1986) X-wing aircraft circulation control. US Patent 4,573,871, March 1986.

13 http://www.rdmag.com/News/2010/01/Energy-More-power-circulation-control-to-alter-wind-turbine-design (accessed august 2010).

14 Lewis, R.I. (1991) *Vortex Element Methods for Fluid Dynamic Analysis of Engineering Systems*, Cambridge University Press, Cambridge, p. xix.

15 Windblat Enercon House Magazine, Issue 3 2008, http://www.enercon.de/www/en/windblatt.nsf/vwAnzeige/4DA5AEEBACEAEDFDC12574A500418221/$FILE/WB-0308-en.pdf (accessed 25 September 2017).

16 Di Maria, F., Mariani, F. and Scarpa, P. (1997) *Chiralic Bladed Wind Rotor Performance*. Proceedings of the 2nd European & African Conference on Wind Engineering, Palazzo Ducale, Genova, Italy, June 1997, pp. 663–670.

17 Holland, R. Jr. (1981) The Holland Roller Windmill. Investigation and Demonstration of Principles. Report No. DOE/R6/10969– T1, DE86 00478, US DOE, June 1981.
18 http://en.wikipedia.org/wiki/Lift_(force) (accessed August 2010).
19 Froude, R.E. (1889) On the part played in propulsion by differences in fluid pressure. *Transactions of the Institute of Naval Architects*, **30**, 390–405.
20 Bergey, K.H. (1979) The Lanchester-Betz limit. *Journal of Energy*, **3**, 382–384.
21 van Kuik, G.A.M. (2007) The Lanchester–Betz–Joukowsky limit. *Wind Energy*, **10** (3), 289–291.
22 Okulov, V.L. and van Kuik, G.A.M. (2011) The Betz-Joukowsky limit: a contribution to rotor aerodynamics by two famous scientific schools. *Wind Energy*, **15** (2), 335–344. doi: 10.1002/we.464
23 Van Kuik, G.A.M. and Lignarolo, L.E.M. (2015) Potential flow solutions for the energy extracting actuator disc flows. *Wind Energy*, **19** (8), 1391–1406.
24 McLaren-Gow, S., Jamieson, P. and Graham, J.M.R. (2013) *An Inviscid Approach to Ducted Turbine Analysis. June 2014*. European Wind Energy Conference & Exhibition 2013: Proceedings of a meeting held 4–7 February 2013, Vienna, Austria, New York, Vol. 1, pp. 931–938.
25 Greet, R.J. (1980) Maximum windmill efficiency. *Journal of Applied Physics*, **51** (9), 4680–4681.
26 Rauh, A., Seelert, A. and Betz, W. (1984) Optimum efficiency for windmills. *Applied Energy*, **17**, 15–23.
27 Sharpe, D.J. (2004) A general momentum theory applied to an energy-extracting actuator disc. *Wind Energy*, **7**, 177–188. doi: 10.1002/we.118
28 Sørensen, J.N. (2016) *General Momentum Theory for Horizontal Axis Wind Turbines*, Springer International Publishing, Switzerland, p. 23.
29 Phillips, D.G., Flay, R.G.J. and Nash, T.A. (1999) Aerodynamic analysis and monitoring of the Vortec 7 Diffuser-Augmented wind turbine. *IPENZ Transactions*, **26** (1), 13–19.
30 Ohya, J. and Karasudani, T. (2010) A shrouded wind turbine generating high output power with Wind-lens technology. *Energies*, **3**, 634–649. doi: 10.3390/en3040634
31 Werle, M.J. and Presz, W.M. (2008) Ducted wind/water turbines and propellers revisited. *Journal of Propulsion and Power*, **24** (5), 1146–1150.
32 McLaren-Gow, S., Jamieson, P. and Graham, J.M.R. (2013) *A Comparison Between Ducted Turbine Theory and Inviscid Simulation*. 2nd IET Renewable Power Generation Conference (RPG 2013), November 2013, pp. 1–44.
33 Oman, R.A., Foreman, K.M. and Gilbert, B.L. (1975) *A Progress Report on the Diffuser Augmented Wind Turbine*. 3rd Biennial Conference and Workshop on Wind Energy Conversion Systems, Washington, DC.
34 Hansen, M.O.L., Sorensen, N.N. and Flay, R.G.J. (1999) *Effect of Placing a Diffuser Around Wind Turbine*. European Wind Energy Conference, pp. 322–324.
35 van Bussel, G.J.W. (2007) The science of making more torque from wind: diffuser experiments and theory revisited. *Journal of Physics: Conference Series, Denmark*, **75**, 1–11.
36 Jamieson, P. (2008) Generalised limits for energy extraction in a linear constant velocity flow field. *Wind Energy*, **11** (5), 445–457.

37 Lawn, C.J. (2003) Optimisation of the power output from ducted turbines. *Proceedings of the Institution of Mechanical Engineers, Part A: Journal of Power and Energy*, **217**, 107–117.

38 http://www.flodesignwindturbine.org (accessed August 2010).

39 Jamieson, P. (2008) *Beating Betz–Energy Extraction Limits in a Uniform Flow Field*. EWEC 2008, Brussels, March 2008.

40 Glauert, H. (1963) Airplane propellers, in *Division L. of Aerodynamic Theory*, vol. **IV** (ed. W.F. Durand), Dover Publications, New York.

41 Wilson, R.E., Lissaman, P.B.S. and Walker, S.N. (1976) *Applied Aerodynamics of Wind Power Machines*, University of Oregon.

42 Walker, S.N. (1976) Performance and optimum design analysis/computation for propeller-type wind turbines. PhD thesis. Oregon State University.

43 Manwell, J.F., McGowan, J.G. and Rogers, A.L. (2008) *Wind Energy Explained*, John Wiley & Sons, Ltd, Chichester. ISBN: 13: 978-0-471-49972-5 (H/B)

44 van Kuik, G.A.M., Sørensen, J.N. and Okulov, V.I. (2015) Rotor theories by Professor Joukowski: momentum theories. *Progress in Aerospace Sciences*, **73**, 1–18.

45 Whelan, J., Thomson, M., Graham, J.M.R. and Peiro, J. (2007) *Modelling of Free Surface Proximity and Wave Induced Velocities Around a Horizontal Axis Tidal Stream Turbine*. Proceedings of the 7th European Wave and Tidal Energy Conference, Porto, Portugal.

46 Betz, A. (1927) NACA Technical Memorandum 474. Die Naturwissenschaften, Vol XV, No 46, November 1927.

47 Goldstein, S. (1929) On the vortex theory of screw propeller. *Proceedings of the Royal Society of London Series A*, **123**, 440–465.

48 Gasch, R. and Twele, J. (2002) *Power Plants: Fundamentals, Design, Construction and Operation*, Chapter 8,, James & James, ISBN: 10: 1902916379, ISBN: 13: 978–1902916378.

49 Burton, A., Sharpe, D., Jenkins, N. and Bossanyi, E.A. (2004) *Handbook of Wind Energy*, John Wiley & Sons, Ltd, Chichester.

50 De Vries, O. (1979) *Fluid Dynamic Aspects of Wind Energy Conversion*, AGARDograph, vol. **243**, NATO, Advisory Group for Aerospace Research and Development, ISBN: 92 835 1326–6.

51 Jamieson, P. (2009) *Lightweight High Speed Rotors for Offshore*, EWEC Offshore, Stockholm.

52 Spera, D.A. (ed.) (2009) *Wind Turbine Technology: Fundamental Concepts in Wind Turbine Engineering*, 2nd edn, ASME Press.

53 Maheri, A. (2006) Aero-structure simulation and aerodynamic design of wind turbines utilising adaptive blades. PhD thesis. Faculty of Computing, Engineering and Mathematical Sciences, UWE, Bristol.

54 Milborrow, D. (1982) Performance blade loads and size limits for horizontal axis wind turbines. Proceedings of the 4th BWEA Wind Energy Conference, Cranfield BHRA.

55 Boeing (1982) Mod-2 Wind Turbine System development Final Report, Vol. II. Detailed Report No. NASACR-168007, DOE/NASA/0002-82/2, NASA Lewis Research Centre, Cleveland, OH.

56 Snel, H. (2003) Review of aerodynamics for wind turbine. *Wind Energy*, **6** (3), 203–211.

57 Chaviaropoulos, P.K. and Voutsinas, S.G. (2013) *Moving Towards Larger Rotors – Is That a Good Idea?* EWEA Conference 2013, Vienna.

58 Deliverable 2.11. New Aerodynamics rotor concepts specifically for very large offshore Wind turbines http://www.innwind.eu/publications/deliverable-reports (accessed 25 September 2017).

59 Madsen, H.A., Mikkelsen, R., Øye, S. *et al.* (2007) A detailed investigation of the Blade Element Momentum (BEM) model based on analytical and numerical results and proposal for modifications of the BEM model. The Science of Making Torque from the Wind. *Journal of Physics: Conference Series*, **75**, 012016.

60 Madsen, A., Bak, H., Døssing, M. *et al.* (2010) Validification and modification of the blade element momentum theory based on comparisons with actuator disc simulations. *Wind Energy*, **13** (4), 373–389.

61 http://www.gereports.com/post/120795016210/how-does-a-wind-turbine-work-with-ges-new/as (viewed February 2017).

62 Kress, C., Chokani, N., Abhari, R.S. *et al.* (2016) Impact of flow inclination on downwind turbine loads and power, The Science of Making Torque from Wind (TORQUE 2016). *Journal Physics, Conference Series*, **753**, 022011. doi: 10.1088/1742-6596/753/022011

63 Réthoré, P.-E., Zahle, F., Sørensen, N.N. and Johansen, J. (2008) *Comparison of An Actuator Disc Model with Full Rotor CFD Model Under Uniform and Shear Inflow Condition*. 4th PhD Seminar on Wind Energy in Europe: Book of Abstracts, The European Wind Energy Association, pp. 125–126.

64 Shen, W.Z., Mikkelsen, R. and Sorensen, J.N. (2005) Tip loss corrections for wind turbine computations. *Wind Energy*, **8**, 457–475. doi: 10.1002/we.153

65 Anderson, M.B. (1981) An experimental and theoretical study of horizontal axis wind turbines. PhD thesis. Cambridge University, Cambridge, UK.

66 Johansen, J., Madsen, H.A., Gaunaa, M. *et al.* (2009) Design of a wind turbine rotor for maximum aerodynamic efficiency. *Wind Energy*, **12** (3), 261–273. doi: 10.1002/we.292

67 Glauert, H. (1926) A General Theory of the Autogyro. ARCR R&M No.1111.

68 Kloosterman, M.H.M. (2009) Development of the Near Wake behind a HAWT including the development of a free wake lifting line code. MSc thesis. TU Delft.